Materials Research
Express

ACCEPTED MANUSCRIPT • OPEN ACCESS

Hybrid Biochar-Graphitic Carbon Nitride (g-C_3N_4) composite Photocatalyst: A Facile Strategy for Enhanced degradation of Ciprofloxacin (CIP)

To cite this article before publication: Ijlal Idrees *et al* 2025 *Mater. Res. Express* in press https://doi.org/10.1088/2053-1591/adb9bc

Hybrid Biochar-Graphitic Carbon Nitride (g-C_3N_4) composite Photocatalyst: A Facile Strategy for Enhanced degradation of Ciprofloxacin (CIP)

Ijlal Idrees[1,†], Muhammad Zafar[2,†], Malik Adeel Umer[3], Amna Mir[4], Fahad Rehman[1], Abrar Faisal[1], Abdul Razzaq[1,*],Woo Young Kim[5,*]

[1] Department of Chemical Engineering, COMSATS University Islamabad, Lahore 54000, Pakistan

[2] Institute of Energy and Environmental Engineering, University of the Punjab, Lahore 54590, Pakistan

[3] School of Chemical and Materials Engineering (SCME), National University of Sciences and Technology (NUST), H-12, Islamabad 44000, Pakistan

[4] Department of Physics, COMSATS University Islamabad, Lahore 54000, Pakistan

[5] Department of Electronic Engineering, Faculty of Applied Energy System, Jeju National University, Jeju-si 63243, Jeju Special Self-Governing Province, Korea

[*] Authors to whom correspondence should be addressed.
A. Razzaq : abdulrazzaq@cuilahore.edu.pk
W. Y. Kim : semigumi@jejunu.ac.kr

[†] These authors contributed equally to this work.

Abstract

Amongst the diversity of pharmaceutical micropollutant degradation methods and to counter the possible hazards posed by these micropollutants economically and sustainably, a new approach of wastewater treatment involving advanced oxidation process (AOP) like photocatalysis offers a viable and economical treatment of micropollutants in wastewater. Amongst a variety of photocatalysts, the one that emerged as the most economical, abstemiously thermally stable, innocuous, and resourceful semiconductor photocatalyst is graphitic carbon nitride (GCN). Hence, bearing in mind these aspects together with the simplistic preparation approach and visible light absorption of GCN, a composite of GCN with Biochar (BC) is prepared in this contemporary research work aiming towards enhanced degradation of Ciprofloxacin (CIP) through improved visible light absorption and good photoexcited electron-hole separation. The enhancement in the photocatalytic activity of GCN is achieved by changing the quantity of BC. This alteration in BC content led to the creation of an optimum sample with the best degradation efficiency towards CIP. The superlative removal efficiency with 75% removal of CIP was exhibited by the 0.22-BGCN sample whose removal efficiency was noted to be 3.5 times higher than GCN (21%). These results point towards the success of composite formation of GCN with BC due to enhanced photocatalytic activity observed in the results and prove the creation of a visible light active (VLA) photocatalyst for efficient removal of pharmaceutical micropollutants like CIP from wastewater. Many different methods are employed to study the physiochemical, textural, and optical properties of the prepared material which include Brunauer–Emmett–Teller (BET) surface area, X-ray diffraction spectroscopy (XRD), Scanning electron microscopy (SEM), Fourier Transform Infrared (FTIR) spectroscopy, UV Visible absorption, and Photoluminescence (PL) spectroscopy.

Keywords: Composite Photocatalyst, Biochar, Graphitic carbon nitride (GCN), Visible Light activity, Ciprofloxacin (CIP), degradation, removal

1. Introduction

Pharmaceutical products are used abundantly in everyday life to prevent and treat diseases mainly found in humans and animals. However, with the prevention and treatment of diseases, the inappropriate disposal of such pharmaceutical products is also polluting the environment at an enormous level. The presence of such products at a micro-level in our environment has raised deep concerns as they are causing damage to the aquatic ecosystem and are difficult to remove due to inadequate treatment technologies [1]. Among the pharmaceutical products, antibiotics, commonly and excessively used, are posing a threat to millions of people and aquatic ecology due to antibiotic contamination of fresh surface and groundwater [2]. Antibiotics in contact with the aquatic system can react with the local bacterial communities and change the microbial balance and genetics of that ecosystem promoting microbial resistance. Further, the environmental pollution caused by antibiotics has mainly caused the spread of antibiotic-resistant genes and bacteria [3]. WHO's recent report also points towards the statistic that excess consumption of antibiotics favors the development of antibiotic-resistant pathogens (ARP). Pandemics are the main cause behind the spread of these ARPs due to the vast usage of life-saving drugs mainly antibiotics. Another report based on studies in Wuhan, China also suggested that almost 70% of patients were treated with antibiotics during COVID-19 [4]. It is reported that global consumption of antibiotics is estimated to increase up to 200 % by the year 2030 from 65 % in the year 2000, which may lead to severe hazardous environmental pollution influencing mainly human beings and animals.

Among a variety of antibiotics, Ciprofloxacin (CIP) is one of the most detected antibiotic [5]. CIP has been established as the new emerging genotoxic pollutant that is damaging the ecosystem and human health through its long-lasting and severe toxicity [6,7]. To counter its effects on water bodies, some treatment methods are suggested in subsequent research including the

electrochemical method, membrane process, and advanced oxidation process (AOP) [8]. Under the domain of AOP treatment methods, photocatalytic pollutant degradation is considered a convenient and economical approach for degrading the pollutants completely or partially into harmless products/less harmful intermediates [9,10]. The Photocatalytic pollutants degradation approach employs a photocatalyst, which under light irradiation (a cost-effective and clean energy source) proceeds chemical reactions with species, on its surface and/or in the surrounding medium [11]. Overall, the photocatalysts absorb light and generate photoexcited charges (electron-hole pairs). These photoexcited charges generation and separation with efficient diffusion to the reaction sites finally degrade the pollutant into harmless or less harmful products. Hence, limitations like optical absorption, low surface area, high recombination of photoexcited charges, and inefficient diffusion to the surface are critical to photocatalytic performance and require to be addressed efficiently [12,13]. Hence, the importance of developing a photocatalytic approach countering the mentioned restrictions is imperative for the scientific community involved in the respective research area. Until today several approaches have been investigated with the objectives of enhanced photocatalytic performance such as doping [14], heterojunction such as p-n junction and z-scheme formation [15,16], nanostructured photocatalysts [17] and composite photocatalysts [18] with a variety of based materials etc. Another influential approach is the selection and moderation of a photocatalyst that is easy to synthesize, non-toxic, harmless, and most importantly bears a moderate band gap that is active toward visible light [19].

Amongst numerous visible light active photocatalysts, graphitic carbon nitride, g-C_3N_4 (GCN), is considered an advantageous and favorable photocatalyst for a variety of applications. Contrasting TiO_2, which is active under UV light region, GCN holds a bandgap of ≈2.7-2.9 eV, allowing it to absorb visible light to proceed variety of reactions [20]. Furthermore, its polymeric nature permits

variations in its surface chemistry through molecular level surface adjustments, providing adequate flexibility of the edifice, which can aid as a host medium of great compatibility to several inorganic nanoparticles. This concluding feature is greatly valuable for the synthesis of GCN-based composite materials. The exclusive above-mentioned characteristics of GCN brands this compound a highly auspicious photocatalyst for various applications [21]. Despite its favorable aspects, GCN displays major constraints of low surface area and immense photoexcited charges recombination. To overcome the key issues of limited surface area and high charge recombination, several studies have recommended loading photocatalysts on the surface of a high surface area, porous, and active site-rich material. During the last few decades, carbon-based materials such as carbon nanotubes, graphene, reduced graphene oxide, and biochar are considered the finest base materials due to their steady structure, high electron conductivity, and surface area. Moreover, carbon-based composite photocatalysts show increased tendencies toward micropollutant removal from water [22]. Among various porous carbonaceous compounds, biochar (BC) acts as an efficient carbon-based material because of its high surface area, low production cost, porous edifice, and rich functional groups [23]. BC in the application of photocatalysis, is purely used as a sustenance material for the deposition of photocatalytic material due to its high surface area and porous structure with improved stability and photocatalytic activity [24].

In recent years, a lot of investigations have been done to compost biochar with a photocatalyst employed for the degradation of targeted pollutants. Used Tea leaves (UTLs) were used to synthesize BC which is further used to remove CIP from aqueous solutions [25]. Similarly, Photocatalytic oxidation of CIP was studied using TiO_2@g-C_3N_4@BC composite and reported a high oxidation rate [26]. Another study demonstrates the modification of the structure and band gap of GCN, through thermal condensation of melamine in the presence of different mass ratios

of BC and applied for the degradation of Rhodamine and Methyl Orange. The degradation rate of the catalyst for pollutants was reported to be 2.5 and 5 times faster than conventional GCN and good stability was noted for four experimental cycles [27].

The admirable and auspicious aspects offered by biochar inspired us to utilize a composite photocatalyst approach in the present work, using eggshell-derived BC as a base material for the loading of GCN photocatalyst. BC prepared from eggshells offers a low-cost source having a moderate surface area and an easy-to-synthesis approach. Biochar/Graphitic carbon nitride (BGCN) composite photocatalysts thus prepared are expected to offer improved visible light absorbance for effective CIP removal, targeted pollutant. The enhanced photoactivity of the BC and GCN composite can be mainly attributed to the narrowing of the band gap by induced defect states, improved surface area, and minimized charge recombination. Furthermore, the BC content is varied and refined within the composite photocatalyst i.e. BGCN, following CIP photocatalytic degradation. It is presumed that such a simple and facile strategy employing eggshell-derived biochar for CIP degradation offers an alluring and uncomplicated way for the development of composite photocatalysts with bettered properties and performance.

2. Materials and Methods

2.1. Chemicals for analysis

Urea ($NH_2CONH_2 \geq 99\%$) is used without further modifications and is purchased from PENTA CHEMICALS (PVT) LTD. Biochar is prepared on a lab scale using waste eggshells through the pyrolysis method. Biopak Polisher's water purification assembly is used to obtain deionized water (DI) which is used for washing and as a solvent during the complete experimentation process. The target micropollutant in this study is Ciprofloxacin (CIP) antibiotic which is bought from ADAMJEE Pharmaceuticals (PVT) LTD. Ethylenediaminetetraacetic acid (EDTA anhydrous ≥98%), Isopropyl alcohol (IPA, natural ≥98% FG), and ethanol (≥99.5% ACS reagent)were procured from Sigma-Aldrich for scavenger experiments and were used without any modifications..

2.2. Experimental preparation of GCN

The thermal polycondensation process was used for the preparation of GCN. Briefly, a 100 ml ceramic crucible was filled with 20 g urea. This ceramic crucible was placed in a muffle furnace which was then operated for 3 h at 550°C in static air. Upon completion of the thermal polycondensation process in the muffle furnace, a mild-yellow color powder was obtained which was removed from the furnace and crushed via mortar and pestle. This powder was then washed three times using a vacuum filtration assembly and desiccated overnight in a drying oven at 70 ˚C. The prepared product was termed "GCN".

2.3. Synthesis of Biochar

Biochar was produced as reported [28] by the pyrolysis method. Waste eggshells were collected, properly washed with DI water, and oven-dried at a temperature of 105℃ in an oven for 24 h. The dried eggshells were ground to a fine powder which was again subjected to dry in an oven at 105 ℃ (overnight) for further removal of any moisture content. The dried crushed eggshells were taken in a ceramic crucible with a tight covering and subjected to pyrolysis in a muffle furnace at 500℃ for 2 h. The resulting black powder product was collected after natural cooling, ground, properly washed, and dried. The final dried product, i.e. biochar is collected and used for composite photocatalyst preparation.

2.4. Synthesis of Biochar/GCN composite (x-BGCN)

Biochar-GCN composite photocatalysts were prepared by simply solid mixing by mixing the specific amount of BC with Urea (GCN precursor) followed by a thermal polycondensation process (as for GCN). The experiment was commenced when 10.0 g urea was added with a quantified volume of biochar (BC) in an agate mortar and ground for 30.0 minutes using a pestle. After proper grinding, a grey color powder was obtained which was taken in an earthenware container. This container was closed tightly and placed in a muffle furnace with similar operating parameters as described in the previous sections. Synthesized semiconductor composite was taken out, crushed, and cleaned by vacuum filtration assembly. This composite was then placed in a drying oven and dried overnight as per the previously mentioned parameters. By changing the volume of biochar (BC) = 0.11g, 0.18g, 0.22g, and 0.53g, four dissimilar composite photocatalysts

were prepared and tested for the enhanced removal of CIP from wastewater. These diverse composites were named "0.11-BGCN, 0.18-BGCN, 0.22-BGCN, and 0.53-BGCN".

2.5. Materials characterization

Fourier transform infrared spectroscopy (FTIR THERMO NICOLET 6700 USA) was used for the determination of organic, inorganic, and polymeric functional groups in the synthesized material. To identify the unique fingerprint and phase composition of a crystal, X-ray diffraction (XRD) graphs of the synthesized samples were obtained by PANalytical X-pert diffractometer, Pro DY38059, using 0.15406 nm Cu Kα particle emission. The surface area of synthesized samples was attained using the Brunauer–Emmett–Teller (BET) technique using Tristar II 3020 (Micromeritics, USA). Before N_2 physisorption, the samples were degassed at a temperature of 200 °C before measurements, and N_2 sorption isotherm was measured at -196 °C. The recombination of photoexcited charges was assessed by RENISHAW UK's Photoluminescence spectrophotometer (PL), with a laser excitation source of 457 nm. The prepared samples' surface morphology was analyzed by gaining pictures on different resolutions from a Scanning electron microscope (SEM) model JSM-6490A. Biotechnology Medical Services (BMS) UV-1602 spectrophotometer showed the light absorbance capability of the synthesized materials in detail.

Tauc's relation was used to study the band gaps (Eg) of synthesized material as per the following relation [18,29]:

$$(\alpha h\nu)^n = A\,(h\nu - Eg) \qquad \text{Eq. 1}$$

α = coefficient of molar absorption

A = constant

Eg = normal band gap of the material

n = number of transitions

hv = energy of photon.

2.6. Analysis of the photocatalytic activity

The activity of the synthesized composites was evaluated by the visible light-assisted removal of CIP from simulated wastewater. The photocatalytic specimens contain GCN, 0.11-BGCN, 0.18-BGCN, 0.22-BGCN, and 0.53-BGCN. Characteristically, a 20-ppm solution of CIP was prepared in 100 ml DI water, and its light absorption range was calculated for the visible light-assisted disintegration contrast of CIP under dark and bright conditions. A glass reactor with 5W LED light and magnetic stirrer was used to house the prepared CIP solution. After pouring 100 ml of 20 ppm CIP solution into a glass reactor, a 50 mg photocatalyst was added to it. An adsorption-desorption equilibrium was achieved after incessant stirring of this photocatalytic mixture in the dark for 60 minutes. UV-VIS pattern was calculated by taking 15 ml CIP-photocatalyst solution in a tube and centrifugating it for 300 seconds at an RPM of 5000 in a centrifuge. Following separation, 4 ml of clear liquid from the tube was taken in a quartz cuvette for UV-VIS absorption analysis. This method was repeated every 15 minutes for 4 hr when the 5W LED light was initially turned on. The degradation efficiency was calculated with the help of the following equation [30]:

$$\text{Rate of degradation} = \frac{C_0 - C_i}{C_0} \times 100 \qquad \text{Eq. 2}$$

C_0 = primary concentration of CIP at t = 0

C_i = concentration of CIP at a given time

A quasi-first-order kinetic model was used to study the reaction rate of CIP removal. The relation of reaction rate for this type of model is specified as follows [31]:

$$kt = \ln\left(\frac{C_T}{C_o}\right) \quad \text{Eq. 3}$$

C_o = primary concentration of CIP

C_T = concentration of CIP after given time "T".

2.7. Scavenger experiments

Scavenger experiments were performed for identification of reactive oxygen species (ROS) generation during the photocatalytic process. The best photocatalyst sample i.e. 0.22 BGCN was employed for the scavenger experiments. EDTA, IPA, and ethanol were used as scavengers for the identification of ROS like OH• and $O_2^{\bullet -}$. 0.1 M of these scavengers were added in 100 ml of 20 ppm of CIP solution containing 50 mg of photocatalyst sample, all placed in photocatalytic reactor. The scavenger experiment was proceeded in the same manner as the photocatalytic activity evaluation experiment i.e. 60 min. dark experiment followed by light irradiation for 4 h.

3. Results and Discussion

3.1. X-ray diffraction (XRD) spectroscopy

The phase composition and structure of crystals with unique fingerprints in these synthesized specimens were examined with the help of their XRD spectra. The XRD spectra for BC, GCN, and 0.22-BGCN composite (representative biochar-graphitic carbon nitride composite sample) are displayed in Fig. 1. As biochar was synthesized from waste eggshells, its XRD peaks depict the presence of certain minerals along with a major portion of carbon content. It can be observed that BC sample exhibit peaks for Ca $(OH)_2$ at 18.08° depicting low Ca $(OH)_2$ presence in the BC structure whereas the characteristic peaks are around 2θ = 21.08°, 23.4°, 28.24°, 29.74°, 36.32°, 39.76°, 42.66°, 46.02°, 47,86°, 48.84°, 50.38°, 51.44°, 52.72°, 57.94°, 60.16°, 61.16°, 65.08° can be associated to $CaCO_3$ content. The peaks responsible for Dolomite $CaMg(CO_3)_2$ appears around 2θ = 68.48°, 77° while calcite ($CaCO_3$) with Dolomite gives the peaks at 2θ = 70.44°, 73.66°, 75.88° [32,33]. Beyond the smaller peaks of certain minerals, an intense peak appearing around 26.88° and a minor peak around 43.44° indicate 002 plan of crystalline carbon depicting the presence of graphitic structure in biochar [18]. XRD pattern of pure GCN shows two points at 13.38° and 27.86°. The minor point shows 100 planes of organized C-N group, proving the presence of the main GCN structure i.e. nitrogen linked heptazine unit. The loaded crystalline graphitic framework of GCN is shown at 27.86° which is a characteristic plane of GCN i.e. 002. Such peaks for GCN, are suppressed in 0.22-BGCN (representative composite photocatalyst sample) indicating structural deformation of GCN after the addition of BC [34]. The characteristic peak of GCN at 27.86° has two small peaks immersed in it at 27.12° and 29.8°. The peak at 27.12° testifies to the formation of BGCN composite as it indicates the (002) plane which is the graphite-like crystalline surface of biochar that might have slipped out of alignment and immersed in GCN structure [35].

Moreover, the peaks appearing at 27.12°, 29.8° and 60.12° in 0.22-BGCN sample designated 002, 200, and 211 surfaces of graphite which confirms the partial graphitization of material at high temperatures ultimately refining the conductivity of 0.22-BGCN composite [36]. Furthermore, 0.22-BGCN also shows CaO's characteristic peaks (2θ = 39.76°, 55.52°, 57.72°, 68.14°) and Ca $(OH)_2$'s characteristic peaks (2θ = 47.86°, 48.78°). CaO and Ca $(OH)_2$ may provide active sites in the 0.22-BGCN composite for pollutant capturing thus enhancing the removal efficiency of the GCN sample through the addition of BC. It may be predicate here that CaO has been formed by the calcination of $CaCO_3$ present in the 0.22-BGCN composite while Ca $(OH)_2$ is produced in 0.22 BGCN from a part of CaO hydrating with H_2O from the atmosphere [37].

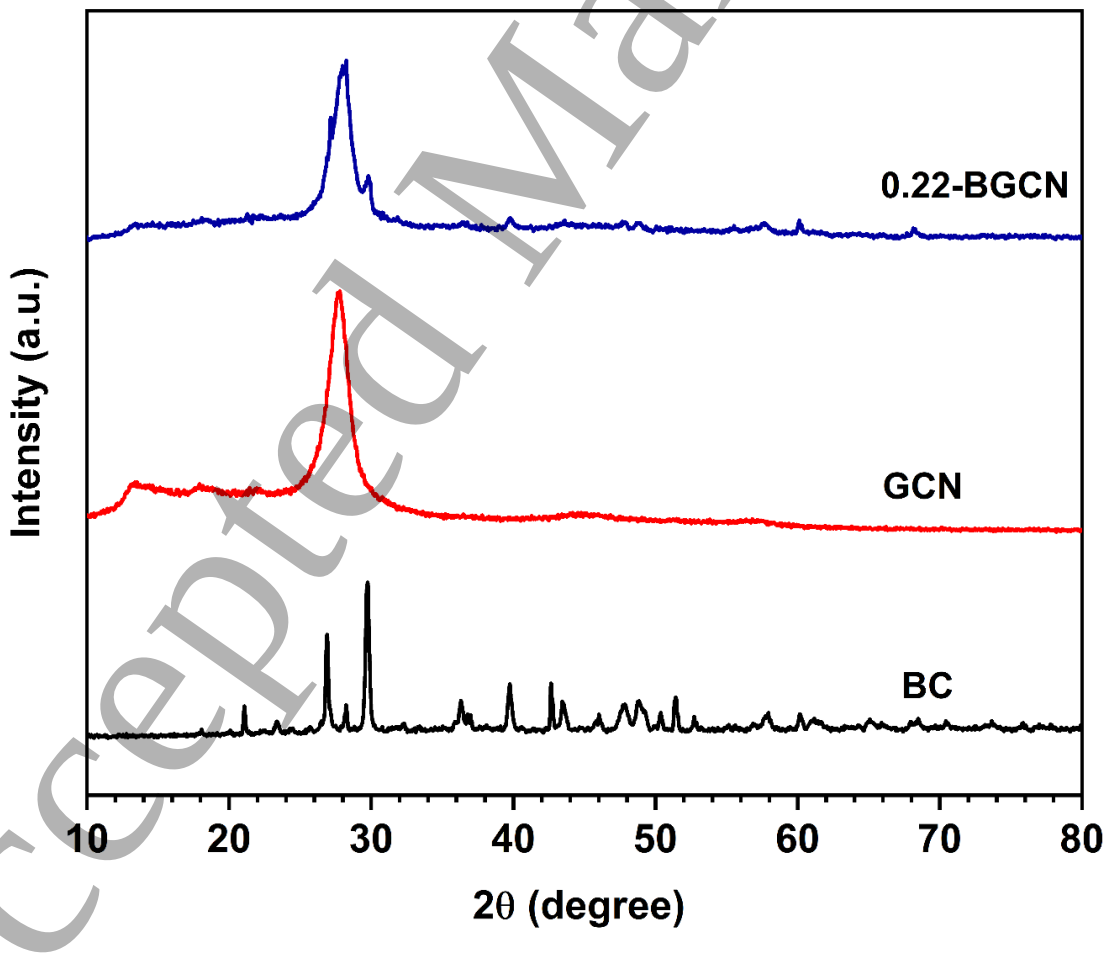

Figure 1. XRD spectral analysis for BC, GCN, and 0.22-BGCN.

3.2. FTIR spectral analysis

The identification and complete study of functional groups for BC, GCN, and *x*-BGCN specimens (0.11-BGCN, 0.18-BGCN, 0.22-BGCN, and 0.53-BGCN) is conducted with the help of FTIR spectral analysis and the spectra are displayed in Fig. 2. A wide pattern is exhibited by the majority of specimens within wavenumber 3050-3400 cm^{-1}. Such a wide band represents elongating vibrations of the N-H and O-H groups. However, for the BC sample, this band is less intense which indicates lower O-H group concentration, and for N-H, negligible partial hydrogenation of nitrogen in BC at the edges of the CN layer in the BC sample [38]. Band appearing at 873 cm^{-1} in all specimens including BC is due to the extending vibrational behavior of the C-C group whereas typical widening of heterocyclic C-N group is detected from 1100-1700 cm^{-1} except BC sample [39].

The BC sample shows a band appearing at 1073 cm^{-1} ascribed to C-O-C elongating vibration proving the successful fabrication of biochar [40]. The band at 712 cm^{-1} is allocated to the proportional extending, asymmetric enlarging, tilted loop twist, and coplanar loop twist of the carbonate group (CO_3^{2-}) showing the successful preparation of BC using eggshells [41,42].

FTIR spectrum of biochar-GCN composite photocatalysts i.e. *x*-BGCN sample at point 802 cm^{-1} depicts strong shaking and torsion phonons of the tri-s-triazine loop (of GCN) [43]. Further, a new peak appearing at 2162 cm^{-1} has been observed in all *x*-BGCN samples. This new point indicates that sp^2 C-N bonds present inside the triazine loop are structurally deformed because of the addition of a specified amount of BC to the GCN structure. It is presumed that this structural distortion favored the creation of new -C≡N bonds, with the highest peak strength for 0.53-BGCN,

and the lowest peak strength for 0.11-BGCN. This structural deformation can be ascribed to the thermal polycondensation of GCN combined with BC, releasing of gases and generation of defect sites [44,45]. Furthermore, for GCN & *x*-BGCN specimens, the existence of sp^3 C-N bonds in the evocative ring framework is evident from points 1226 cm^{-1}, 1398 cm^{-1}, 1454 cm^{-1}, 1532 cm^{-1}, and 1624 cm^{-1} [46,47].

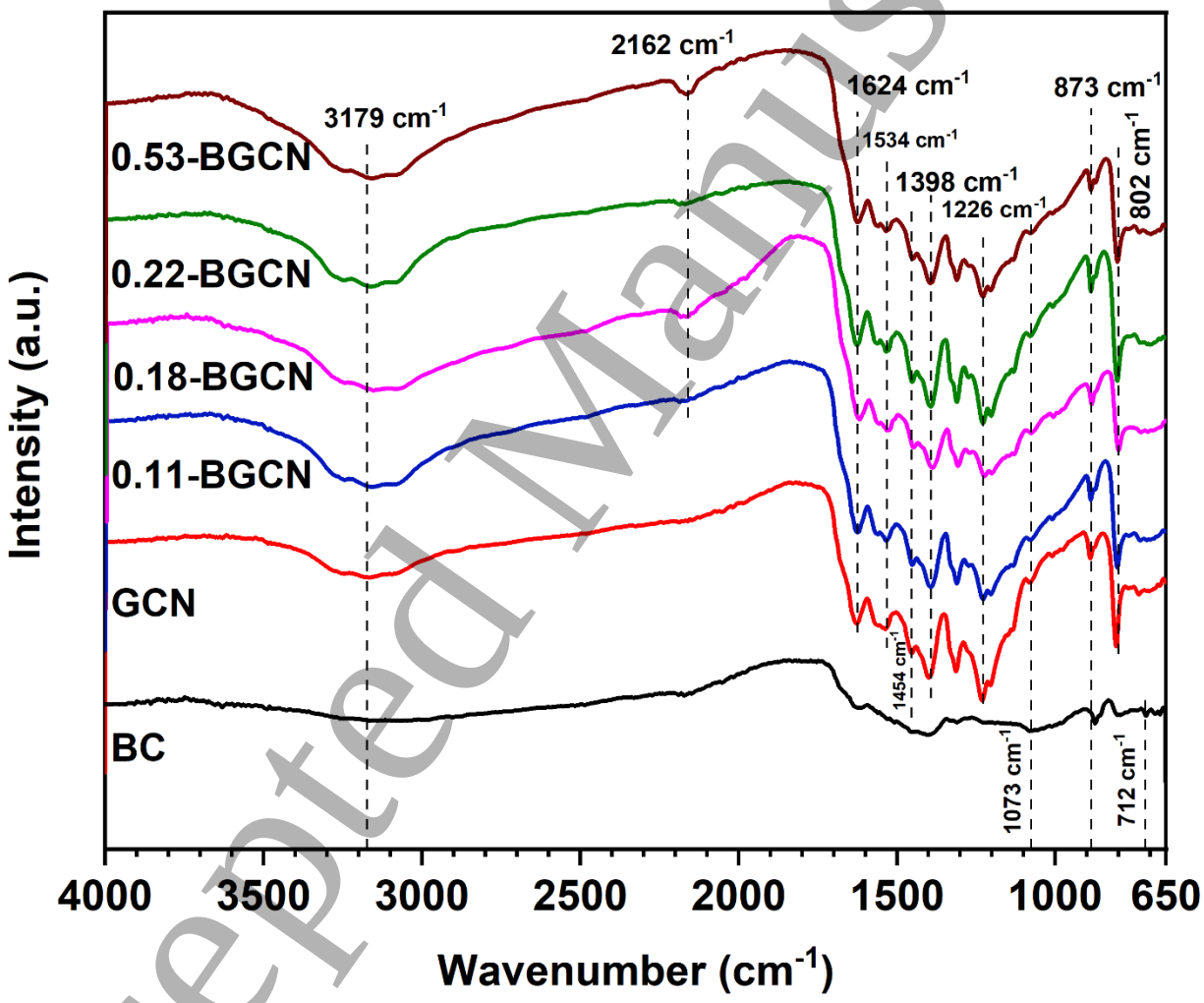

Figure 2. FTIR patterns for BC, GCN, and *x*-BGCN samples (where *x* is 0.11, 0.18, 0.22, and 0.53g BC).

3.3 Scanning electron microscopy (SEM)

The textural and surface properties of BC, GCN, and *x*-BGCN samples (BC fused GCN i.e. *x*-BGCN) are studied by taking pictures of these specimens using scanning electron microscopy (SEM) and is shown in Fig. 3. The surface of the BC sample (Fig. 3a) depicts a flat layered morphology with some pores and crumpled plates merged providing a better surface for pollutant adsorption followed by photodegradation [22,33]. The SEM images of GCN (Fig. 3b), show an asymmetrical, colossal, and roughly agglomerated thin layered stack structure proving a low surface area and dense nonporous structure [48]. However, the composite photocatalysts, *x*-BGCN samples (Fig. 3c-f) show comparative more porous morphology, due to the combined effect of flat surface morphology of biochar and the rough scaly surface of GCN. Moreover, the *x*-BGCN samples also show that as the amount of biochar augments from 0.11 to 0.22 grams, the surface complexity also increases resulting in the intertwining of biochar and GCN layers with each other creating a complex spongy layered structure of the composite with moderate porous morphology up to 0.22-BGCN sample. But as the biochar amount is further increased to 0.53 g, the rough, disorderly, and intertwined layer structure remains the same but with a less porous nature which may be caused by the increased agglomeration of BC on GCN surface [40].

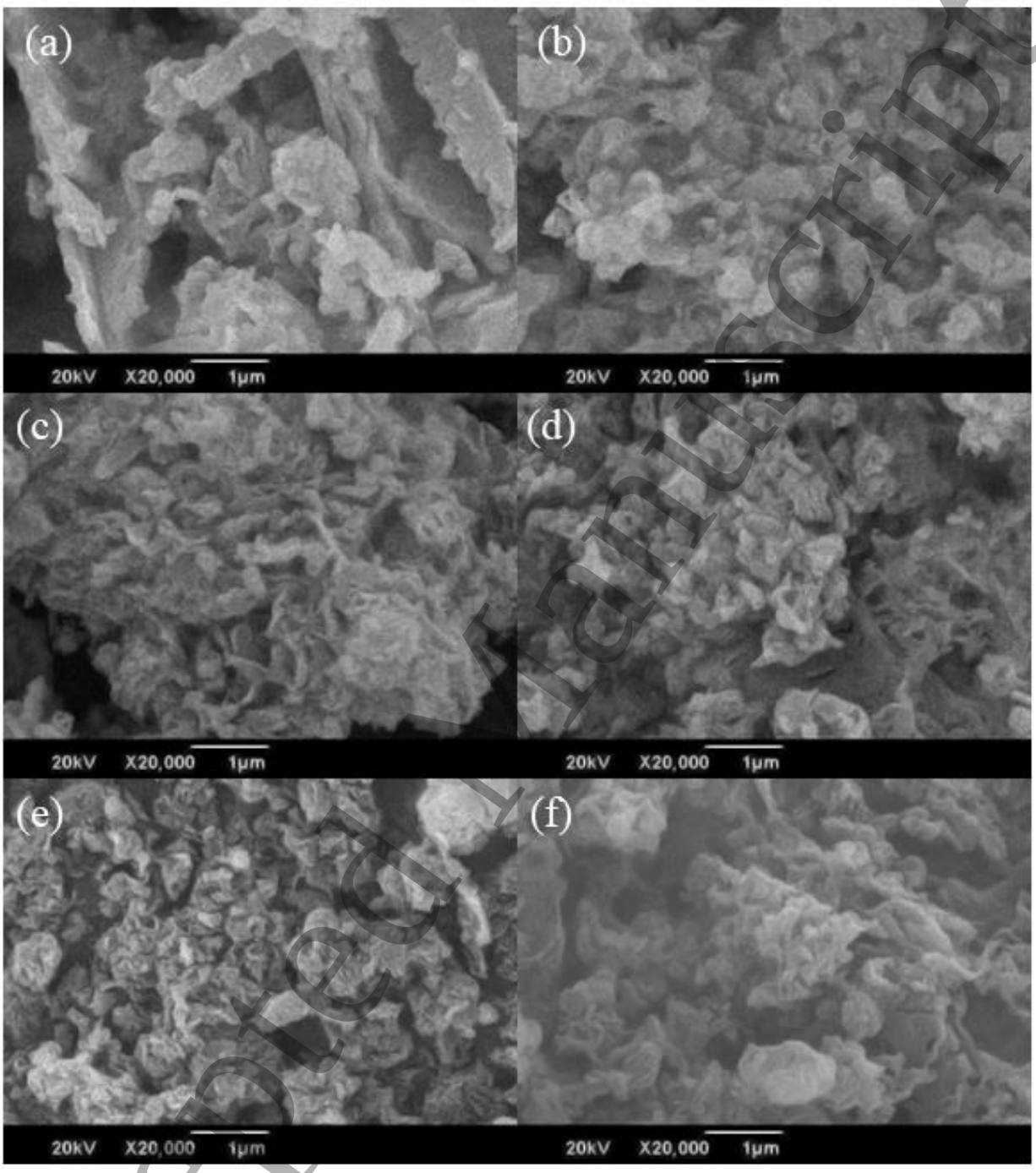

Figure 3. SEM images of (a) Biochar (BC) (b) GCN (c) 0.11-BGCN (d) 0.18-BGCN (e) 0.22-BGCN, and (f) 0.53-BGCN samples.

The atomic concentration (at. %) of three components BC, GCN, and 0.22-BGCN were studied using energy-dispersive X-ray spectroscopy (EDX). The data is given below in Table 1. The data clearly shows the presence of calcium (Ca) in BC and 0.22-BGCN composite samples, further proving the synthesis of biochar using eggshells. The carbon content is also increased in the composite sample as compared with GCN which also supports the successful fabrication of the composite through the inclusion of BC matrix in the structure of GCN.

Table 1. EDX spectroscopy of BC, GCN, and 0.22-BGCN with concentrations in atomic percentage.

	Atomic concentration (at. %)			
Samples	**C**	**N**	**O**	**Ca**
BC	58.80	2.71	26.72	11.71
GCN	36.68	61.08	2.21	0.0
0.22-BGCN	47.56	43.47	8.32	0.61

The textural properties, mainly BET surface area and pore volume were also determined experimentally for BC, GCN, and 0.22-BGCN (representative composite photocatalyst) samples and are provided in Table 2. Pure GCN possesses a lower surface area as compared to pure biochar. However, the composite photocatalyst sample i.e. 0.22-BGCN exhibits higher surface area and pore volume as compared to pure GCN and biochar samples. The surface area of 0.22-BGCN is 9.5 times and 1.8 times higher than GCN and BC, respectively. Such an increase in surface area can be associated with the dissolution of amorphous structure and elimination of impurities within biochar induced by thermal exfoliation during the synthesis of the composite sample in which a

mixture of biochar and urea are subjected to a thermal polycondensation process. With the combination of BC and GCN, there is an increase in the porosity of the composite which increases the surface area of the composite [49]. Also, the sheets of GCN are dispersed due to the presence of BC which reduces the stacking of sheets and maintains an open structure increasing the surface area of the composite [50]. The enhancement in surface area is well in agreement with the reported literature data [51,52]. This increased surface area for the 0.22-BGCN sample may provide more active sites for CIP pollutants to adsorb and react with the oxidizing species produced in a photodegradation process, thus ultimately improving the photocatalytic performance of the composite photocatalyst sample [53].

Table 2. BET surface area and pore volume of BC, GCN, and 0.22-BGCN samples.

Samples	S_{BET} (m^2g^{-1})	Pore volume (cc g^{-1})
Biochar	*79.48*	*0.020*
GCN	*15.96*	*0.0036*
0.22-BGCN	*129.26*	*0.038*

3.4 Analysis of band gap and photonic absorbance

The photonic absorbance spectra analyzed in the case of BC, GCN, and 0.22-BGCN is displayed in Fig. 4. It is noted from the spectra that BC (Fig. 4a) shows an extensive absorption mainly within the visible range, however pure GCN shows an absorption edge appearing around the wavelength of 415 nm [54]. When the GCN is composited with BC, as expected the absorption of the composite photocatalyst is shifted towards the red region. Fig. 4c shows the absorption spectra of the 0.22-BGCN sample stretched in the visible region that consists of wavelength from 400-700 nm. The protracted absorption in the direction of lengthier wavelengths is also termed "redshift" and for the 0.22-BGCN sample it represents the increased visible light absorption capacity of the photocatalyst [55]. This enhancement in the absorption of visible light is ascribed to the addition of BC in the framework of GCN which is already a visible light active photocatalyst to some extent and the addition of BC has caused the structure of GCN to absorb more visible light due to deformed carbon surface of BC that support good light absorption when combined with GCN [27,38].

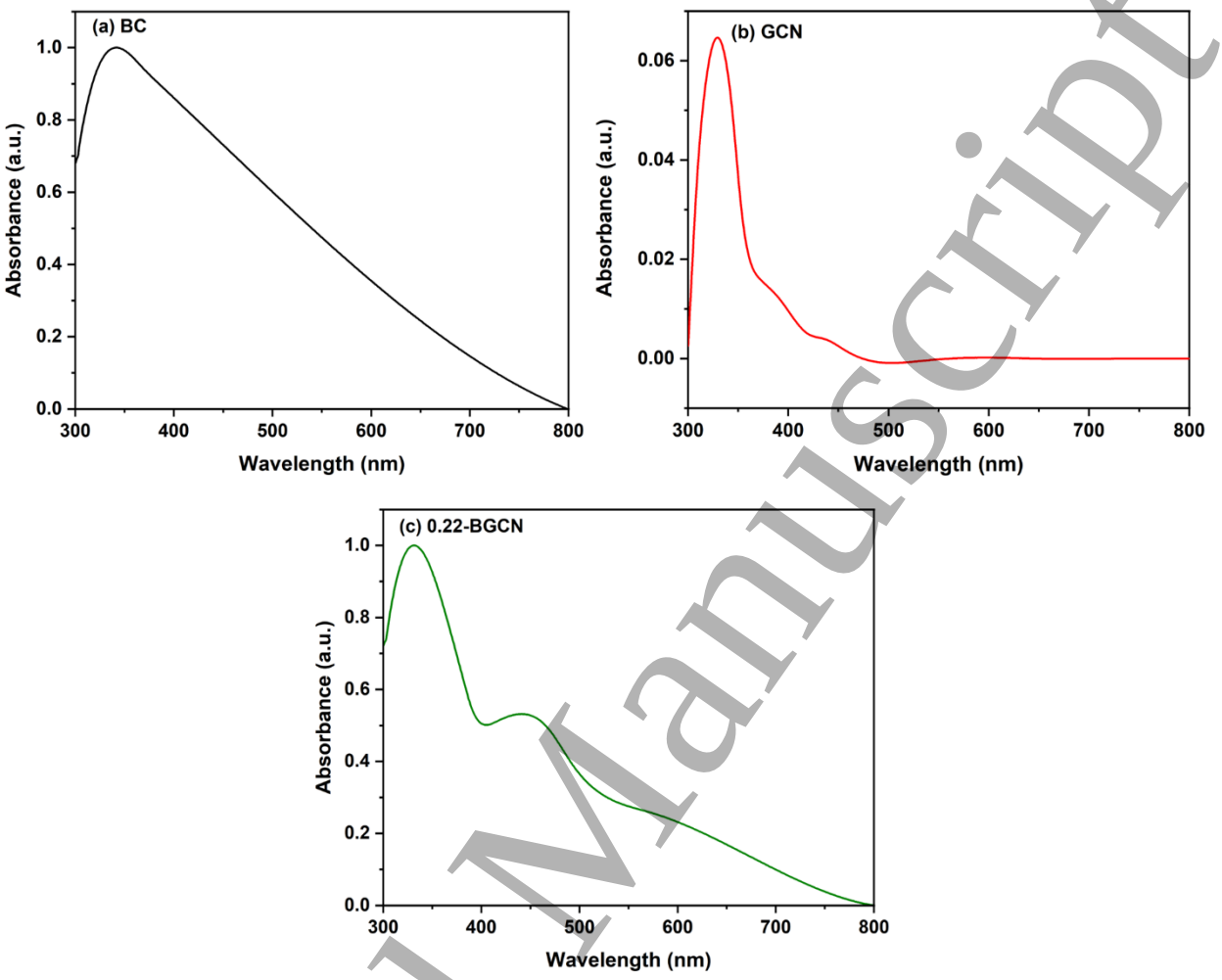

Figure 4. Photonic absorbance pattern for BC, GCN and 0.22-BGCN samples.

With the contemplation of direct band gap value n = 2 in Eq. 1, Tauc's equation was used to assess the band gaps of BC, GCN, and 0.22-BGCN samples. Fig. 5 displays Tauc's plot for GCN and *x*-BGCN samples. For the estimation of the band gap, the linear portion of the plot was extrapolated to the x-axis zero. The direct band gap of GCN is found to be 3.0 [56]. The narrowing of the band gap of GCN is evident in Fig. 5(c) which shows the estimated band gap value for the 0.22-BGCN sample [57]. This information resolutely proposes the creation of defect states in the framework of GCN created by the addition of BC causing the electron to fall back to its valance

shell after an increased amount of time. Moreover, the reduction in band gap is due to in-situ carbon doping in the urea structure during the thermal polycondensation process. This doping of carbon reduces the band gap and allows photons of low energy to be absorbed by the photocatalyst which absorbs light of longer wavelength and generates more electron-hole pairs facilitating and enhancing the degradation process [27]. It further suggests that the addition of dopants on the composite surface can further reduce the band gap inducing improved absorbance and possibly better photocatalytic activity of the catalyst [58].

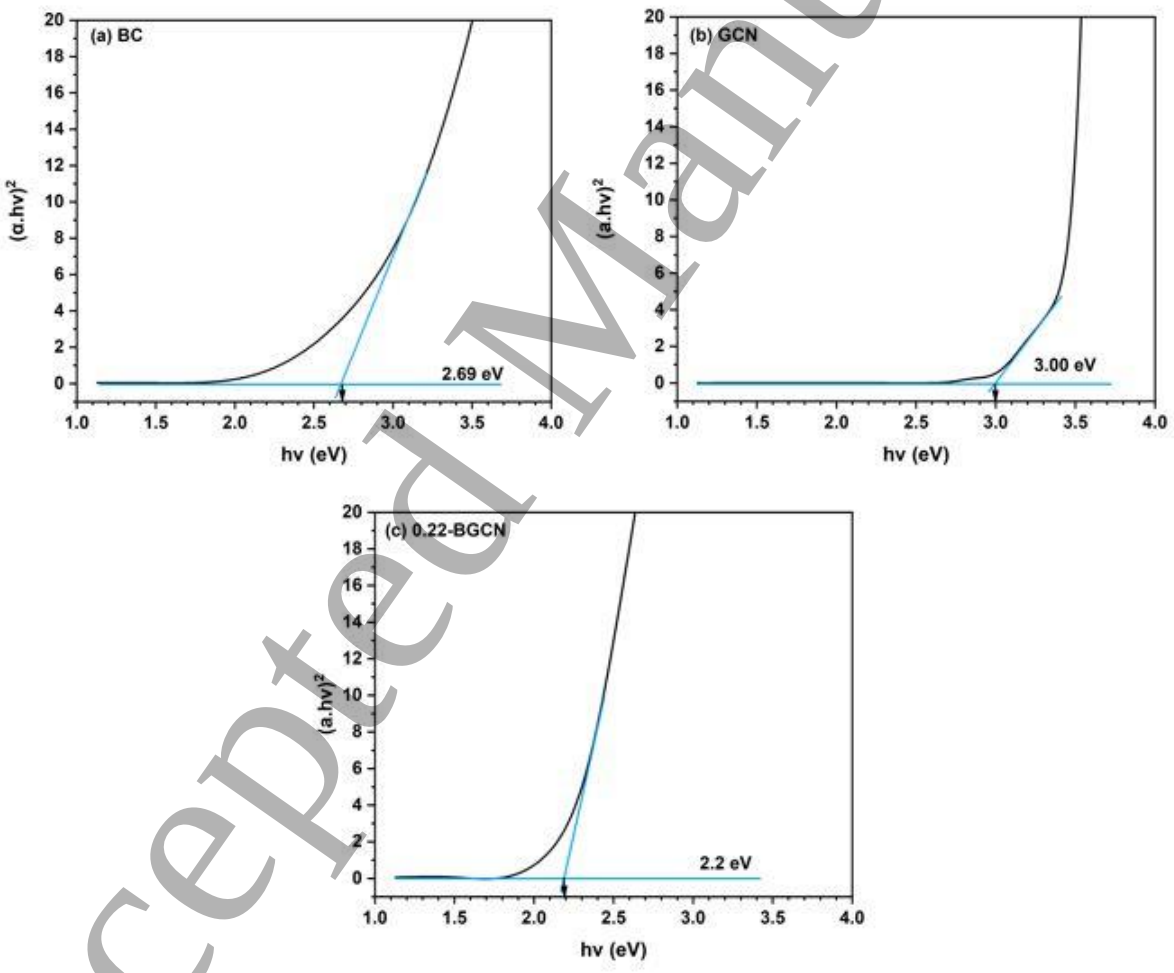

Figure 5. Band gap estimation graph using Tauc's relation for (a) BC, (b) GCN, (c) 0.22-BGCN samples.

3.5 Assessment of Photogenerated charges separation

The separation of photogenerated charges is assessed via Photoluminescence (PL) spectroscopy where an emission spectrum is studied which is created because of electron-hole recombination [59]. Fig. 6 displays PL spectra for BC, GCN, and *x*-BGCN samples. It is clear from Fig. 6a that a solitary emission peak at 620 nm is present in the case of GCN sample, BC (Fig. 6b) peak is around 706 nm, whereas composite specimens i.e. *x*-BGCN specimens: 0.11 BGCN (Fig. 6c), 0.18 BGCN (Fig. 6d) and 0.22 BGCN (Fig. 6e), shows a decreased intensity of PL emission peaks appearing around 575 nm and 706 nm respectively, can be attributed to the quenching of photogenerated electron-holes recombination [60,61]. On the other hand, 0.53 BGCN (Fig. 6f) shows relatively strong PL emission peaks around 590 nm [52]. The valance band (VB) is composed of 2p orbitals of nitrogen whereas the conduction band (CB) comprises of sp^2 hybridized carbon-nitrogen group. For 0.11 BGCN (Fig. 6c), 0.18 BGCN (Fig. 6d), and 0.22 BGCN (Fig. 6e) samples, the initial peak appearing at 575 nm can be associated with the band-to-band recombination, whereas the secondary peak at 706 nm can be associated to the recombination of charges induced by energy levels during composite photocatalyst formation. These energy levels are created by BC's calcite-carbon framework probably below the conduction band. For these mentioned composite samples, it is evident that upon BC addition, the band at 575 nm is reduced slightly, revealing limited radiative recombination of charges. On the other hand, a secondary emission band is formed because of photoexcited electrons extracted at the conductive carbonaceous framework or energy levels formed by BC where they are insnared and recombined after a certain period. Furthermore, it is also observed from PL spectra that the presence of a second peak in 0.53-BGCN is not evident, and the intensity of the peak is comparatively higher. Such behavior can be ascribed to the presence of excessive BC for the 0.53-BGCN sample showing a

similar PL spectrum as that of BC. Consequently, the above interpretation resolutely supports the successful synthesis of BGCN composites and describes it based on the peak intensity reduction of these composites. This reduction in PL peak strength is not evident in the case of GCN. This proves that BC is acting as an electron trapping center resulting in low photoexcited charge recombination. Furthermore, the enhanced reduction of peak strength for 0.18 BGCN and 0.22 BGCN samples (figure 6c-e) is attributed to the creation of an effective BC framework acting as an electron trapping center between these two samples making them optimum samples [53].

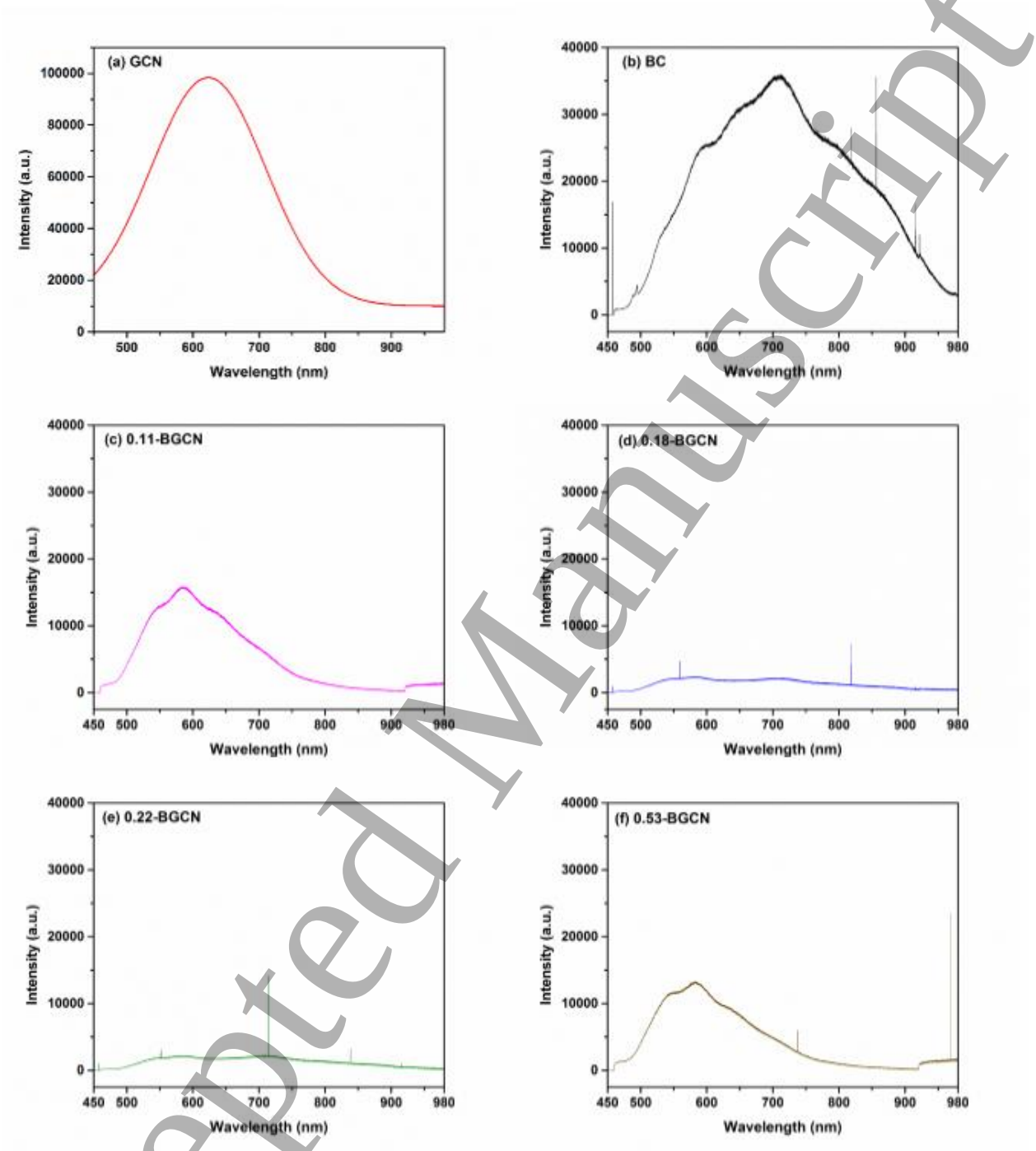

Figure 6. Photoluminescence spectral patterns for (a) GCN, (b) Bio-char (BC), (c) 0.11-BGCN, (d) 0.18-BGCN, (e) 0.22-BGCN and (f) 0.53-BGCN.

3.6 Effect of parameters

The effect of the initial concentration of CIP on its degradation using GCN and optimal sample 0.22-BGCN was studied in this portion. Different initial concentrations of CIP were taken at 10, 20, and 30 ppm. The photocatalyst quantity was 0.05g/100ml and the pH maintained was 7. The photocatalytic degradation of CIP in terms of concentration and rate constant in terms of bar graph was represented in Fig. 7 (a-c) and Fig. 8. It is palpable from these results that by increasing the initial concentration of CIP, the degradation efficiency was reduced for both GCN and 0.22-BGCN samples. As the initial concentration was reduced, the degradation efficiency was enhanced which was the most for 10 ppm concentration. The increase of initial concentration resulted in the enhancement of the number of moles of CIP in the reaction environment which saturated the active sites present on the surface of GCN and 0.22-BGCN catalysts [62]. This reduced the photoactivation of the catalyst surface and reduced the degradation efficiency. Another reason for the reduction in degradation efficiency was the enhanced adsorption of CIP on the surface of the catalyst reducing the light activation or excitation of the photocatalyst surface by decreasing the pathway length of the incoming photons [62].

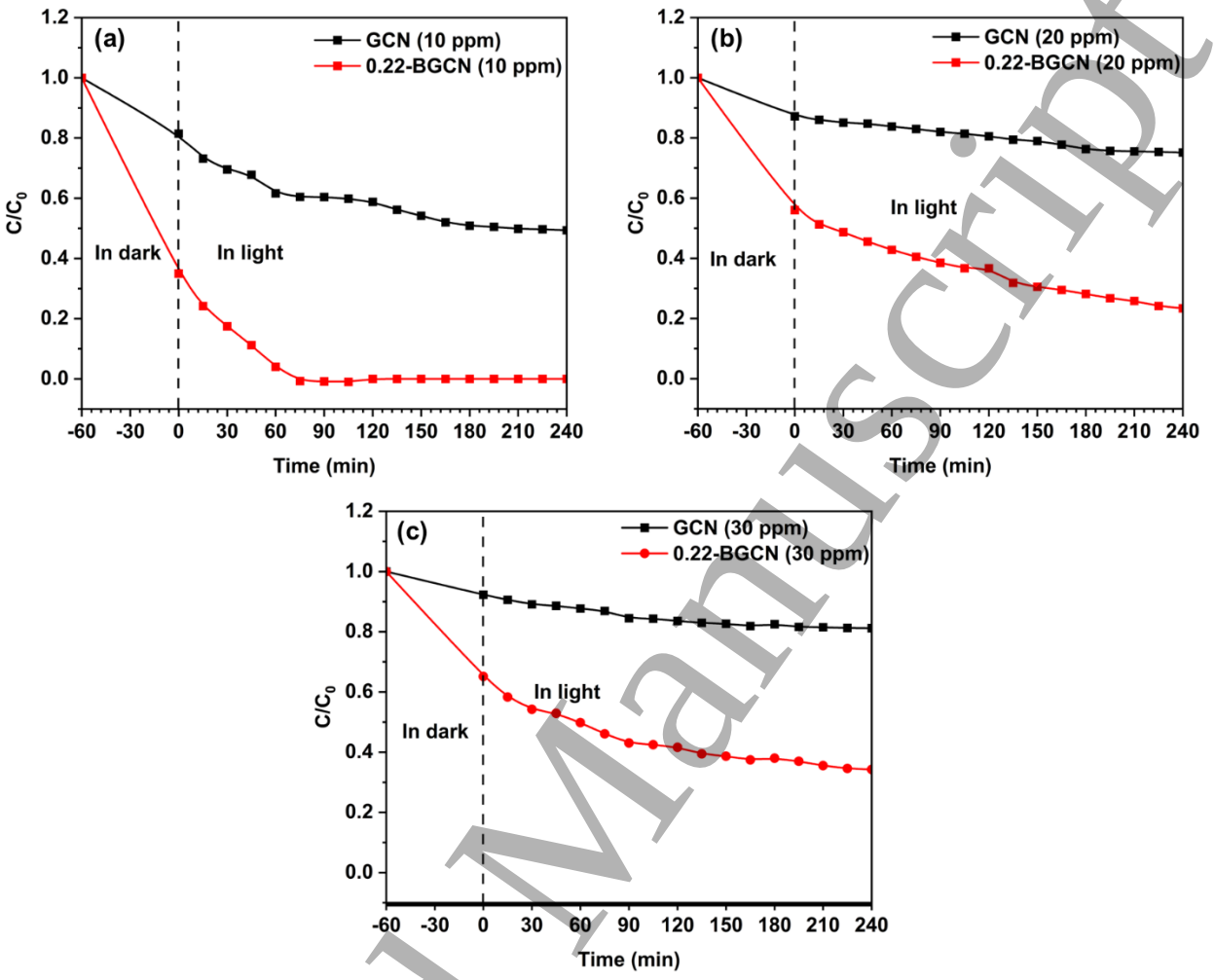

Figure 7. Effect of initial concentration of CIP on degradation efficiency employing GCN and 0.22-BGCN photocatalysts at (a) 10 ppm (b) 20 ppm, and (c) 30 ppm of CIP.

The rate constant (Fig. 8) showed the rate of reaction via pseudo 1st order kinetics and represented a slow reaction rate for a high initial concentration of CIP (30 ppm) and the reaction rate was enhanced as the initial concentration was reduced to 10 ppm. The reason for the reduced reaction rate at elevated concentrations was the same as stated above and was attributed to the increased number of moles of CIP in the reaction medium hindering the photoactivation of the photocatalytic surface [63].

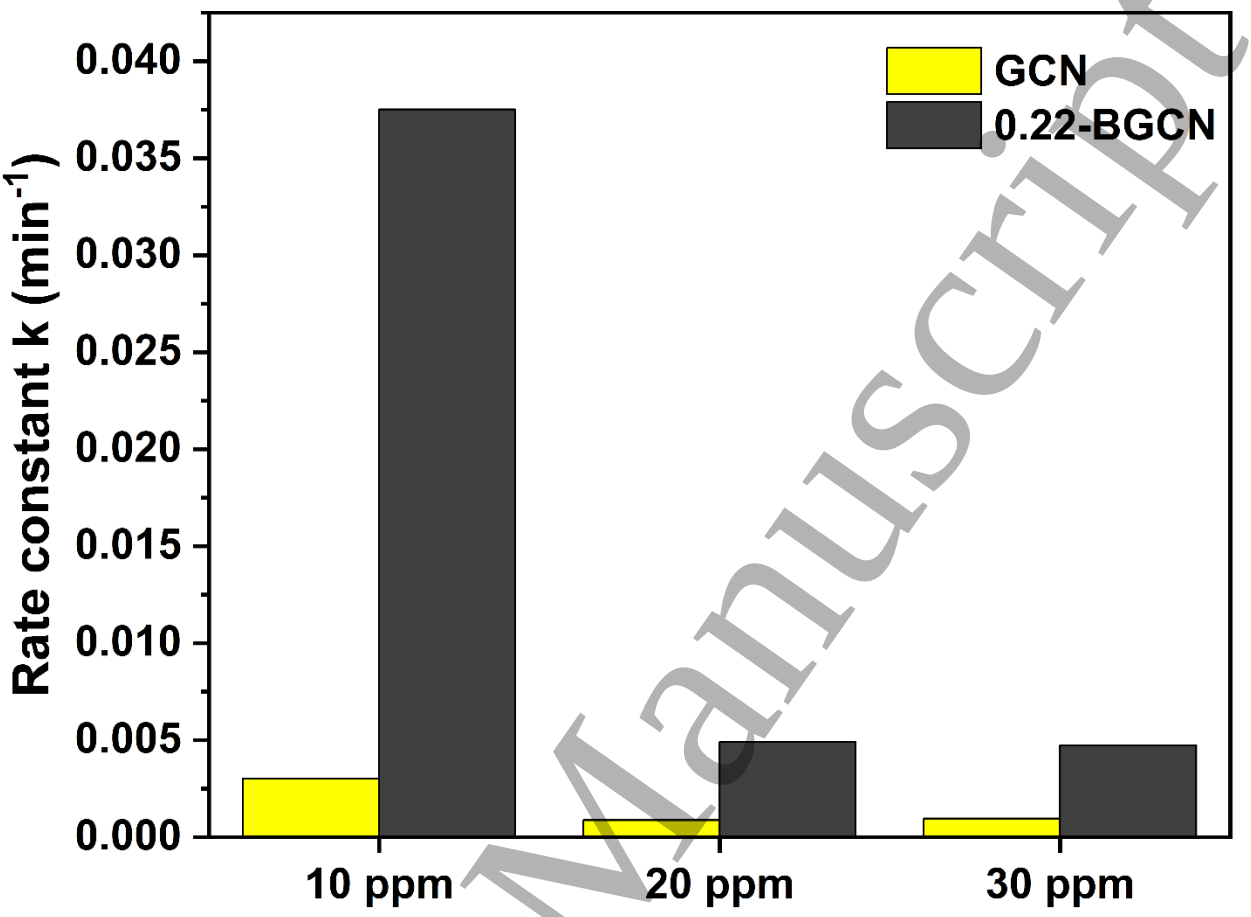

Figure 8. Effect of initial concentration of CIP in terms of rate constant calculated for GCN and 0.22-BGCN photocatalysts.

Below is a table (Table 3) that shows the complete degradation of CIP concerning initial concentration for both GCN and 0.22-BGCN photocatalytic samples.

Table 3. The degradation efficiency of CIP with respect to initial concentration and time for both GCN and 0.22-BGCN samples.

Concentration	Degradation efficiency (GCN)	Time (min)	Degradation efficiency (0.22-BGCN)	Time (min)
10 ppm	*51%*	*240*	*100%*	*90*
20 ppm	*21%*	*240*	*75%*	*240*
30 ppm	*17%*	*240*	*64%*	*240*

The effect of pH on the degradation efficiency of CIP was also evaluated at three different pH levels 5, 7, and 9, and is shown in Fig. 9 (a-c). The concentration of CIP was kept constant at 20 ppm and 0.05 g/100ml catalyst concentration was used. It was observed that under acidic conditions of pH 5, the degradation efficiency was enhanced greatly for both GCN and 0.22-BGCN samples. It was also found that at pH levels of 7, the degradation of CIP was less as compared to the acidic conditions, and at basic conditions of pH 9, the degradation efficiency was more than pH 7 but not more than the acidic pH 5. This is mainly because at acidic pH the surface of the catalyst is negatively charged while CIP has a positive charge on it which attracts the molecule and is adsorbed on the surface of the catalyst, improving the overall efficiency. At neutral pH, there is no charge on the catalyst surface and natural adsorption of CIP occurs. On a pH level of 9, both the CIP molecule and the surface of the catalyst have a positive charge which causes a repulsion effect between the molecule and the surface [62]. Therefore, the adsorption of the pollutant molecule on the catalyst surface is not very efficient under neutral and basic conditions. The

degradation efficiency of CIP under acidic conditions also increased because under acidic conditions the generation of H_2O_2 is enhanced and acidic conditions facilitate its generation as compared to the neutral and basic conditions [64]. H_2O_2 is a very important factor in the degradation of various micropollutants and its amount also decreases as the pollutant concentration decreases in the reaction system [64]. Another factor for the enhanced removal of CIP in acidic conditions is that both OH• and O_2•$^-$ species participate in the degradation of CIP under acidic conditions whereas, under basic conditions, only O_2•$^-$ participates while OH• behaves as a hindering factor reducing the degradation rate or slowing down the reaction rate as compared to acidic conditions [64].

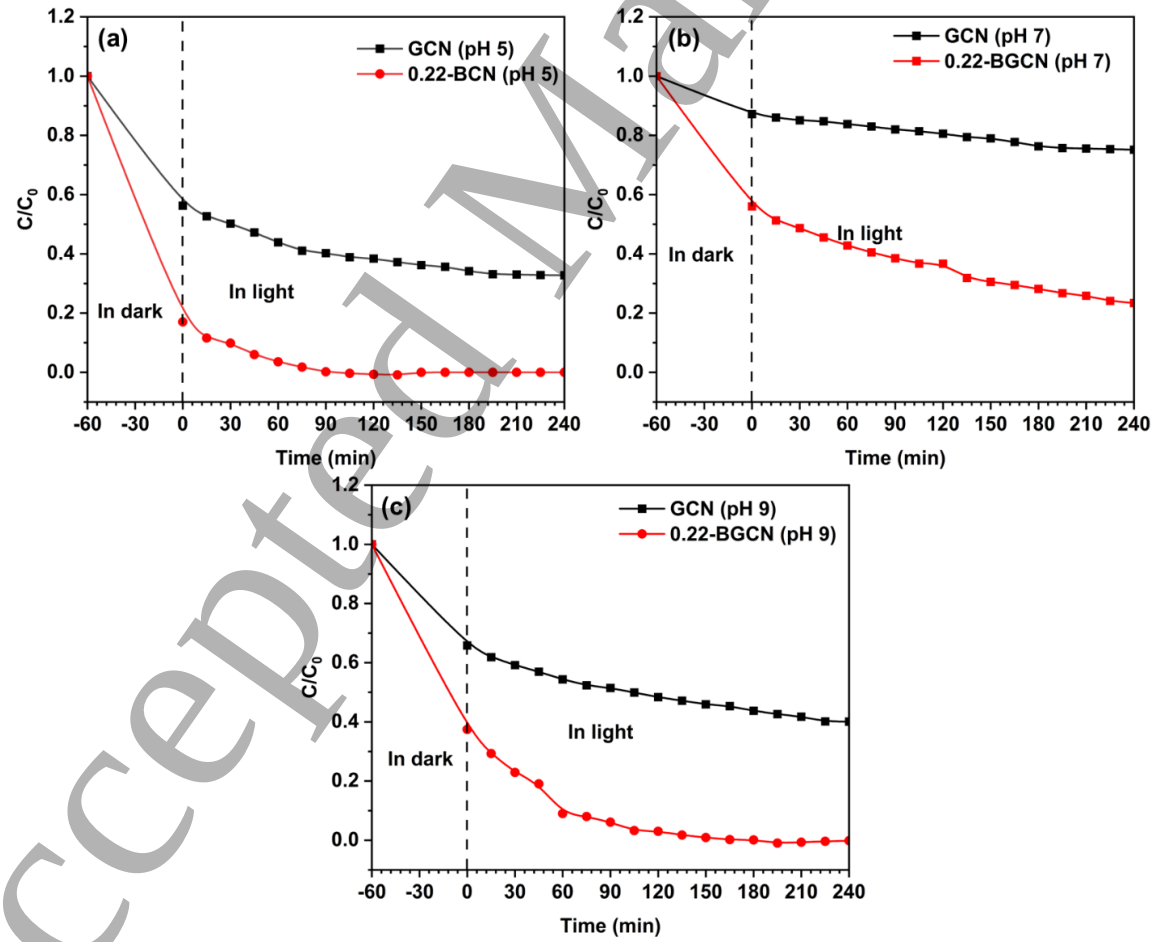

Figure 9. Effect of pH on degradation efficiency of CIP via GCN and 0.22-BGCN photocatalysts at pH levels of (a) 5 (b) 7, and (c) 9.

The rate of reaction was estimated through the calculation of rate constants employing pseudo 1st order kinetics for the degradation of CIP at three pH levels of 5, 7, and 9. The rate constant clearly showed the enhanced rate of reaction at acidic pH (5) followed by a moderate rate of reaction observed for basic pH level (9) and the lowest reaction rate was observed for neutral pH (7). The pH levels showed a trend of CIP degradation under different pH conditions i.e. acidic > basic > neutral [65]. This is shown in Fig. 10 via the calculated rate constant for the degradation of CIP at different pH levels. The degradation efficiency of CIP with respect to time under different pH levels for GCN and 0.22-BGCN samples is also shown in Table 4 below:

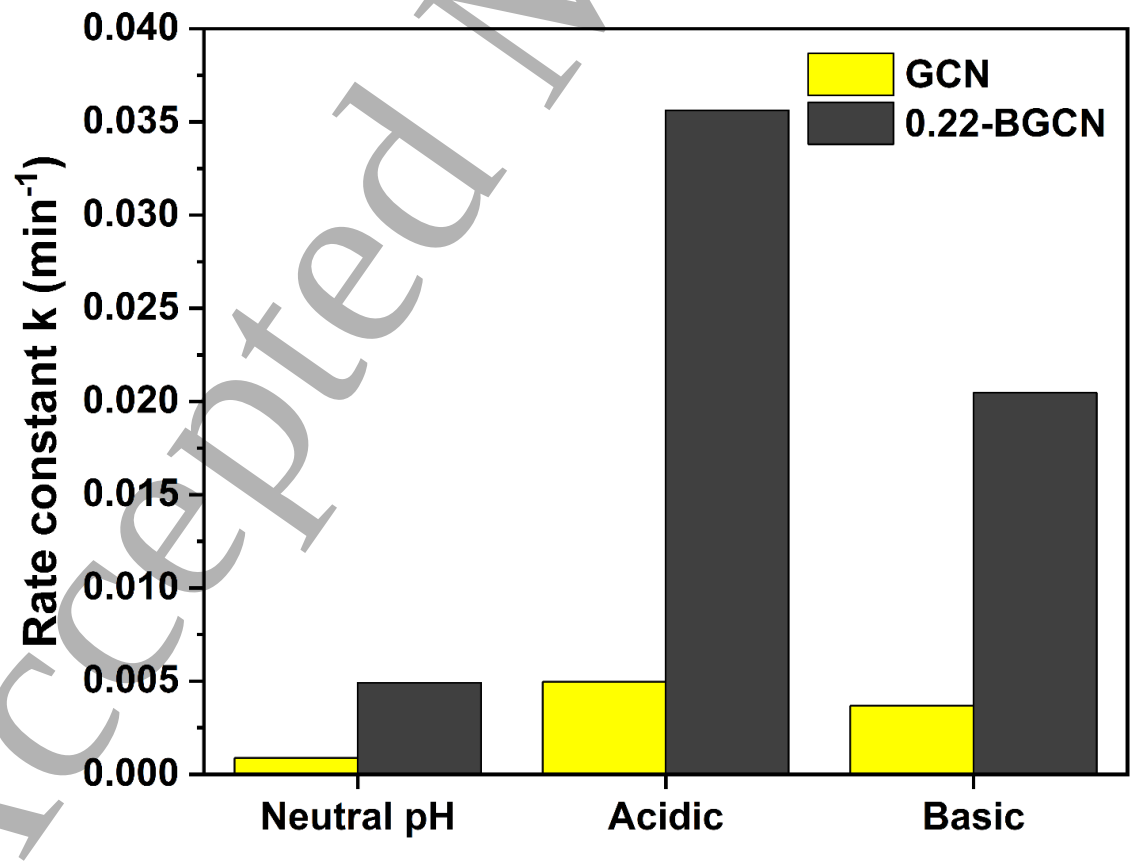

Figure 10. Effect of pH in terms of rate constant on the degradation of CIP using GCN and 0.22-BGCN photocatalysts.

Table 4. The degradation efficiency of CIP with respect to time for both GCN and 0.22-BGCN samples under different pH levels.

pH	Degradation efficiency (GCN)	Time (min)	Degradation efficiency (0.22-BGCN)	Time (min)
5	*67%*	*240*	*100%*	*120*
7	*21%*	*240*	*75%*	*240*
9	*59%*	*240*	*100%*	*210*

3.7 Assessment of the photocatalytic activity

In this section, visible light active removal of CIP from wastewater is assessed to evaluate the performance of prepared composite specimens along with GCN. Equation 2 is used to calculate the concentration profile and removal percentage of CIP pollutant and is displayed in Fig. 11. The experiment consists of two phases i.e. dark and light. Initially, the CIP-composite mixture is stirred in the dark for 1 hr and after this period a deterioration in CIP concentration is observed through a UV-VIS spectrophotometer. This reduction in CIP concentration is only because of adsorption and the purpose of keeping the sample in the dark is to achieve an adsorption-desorption equilibrium through homogeneous dispersion of pollutant in the medium. After the dark phase, white light is turned on and further reduction in CIP quantity is noted which is because of photocatalytic

reactions happening at the surface of the catalyst. The experiment was continued for 4 hr and at the end the most efficiency of degradation (Fig. 11a) and concentration (Fig. 11b) profiles was shown by 0.22-BGCN composite. The degradation and concentration profiles showed a 75% removal rate of CIP. This removal rate of CIP is 3.5 times greater than the 21% removal rate of GCN. Beyond that the photocatalytic efficiency does not increase and the reason for this is photon saturation on the active sites present on the surface of composite photocatalyst, usage of a low energy light source (5W) for degradation experiments, and blockage of some active sites by pore blockage due to carbon deposition [66,67]. The sequence of photocatalytic activity towards CIP pollutant is arranged in the following manner: 0.22-BGCN > 0.18-BGCN > 0.53-BGCN > 0.11-BGCN > GCN. A reduction in the visible light activity was observed for the 0.53-BGCN composite. This reduction in photoactivity is due to the enhanced BC quantity in the sample. This increased BC reduced the light-harvesting of GCN which is necessary for good photocatalytic activity [68]. Equation 3 is used to calculate the rate constant (k) for GCN and x-BGCN composites and is listed in Table 5. Therefore, it is determined that 0.22-BGCN demonstrates superlative photodegradation efficiency. The rate constant also supports this statement and shows the highest value of 0.005 min^{-1} among other specimens.

Improved photodegradation efficiency on the addition of BC is explained on the basis of improvement in optical absorption and electron-hole pair separation [69]. After the addition of BC, redshift was observed in all composite samples which indicated improved visible light absorbance of the prepared samples due to a reduction in band gap [70]. This reduction in band gap is because of energy levels that are trapping electrons and are also causing the photocatalyst to absorb light in the visible region [71]. Simultaneously, the excitation peak in PL patterns is reduced from 0.11 BGCN to 0.22 BGCN (1^{st} peak at 575 nm & 2^{nd} peak at 706 nm). This indicates improved

separation of electron-hole pairs. These electrons are captured by a conductive carbonaceous framework and trapped in the energy state. From these energy states, these electrons are distributed to the surface of the photocatalyst for the removal of CIP. As the quantity of BC is augmented from 0.11 BGCN to 0.22 BGCN, enhancement in photocatalytic performance is detected proving the charge mediator behavior of BC effectively separating electrons and holes with the help of its complex structure and good electrical conductivity. However, upon an additional increase in the BC quantity to 0.53 g, a decline in the visible light activity of the catalyst is perceived. The cause of this decline is elucidated by PL spectroscopy, which shows an increase in the discharge strength of a single excitation peak (590 nm), indicating quick recombination of photogenerated electrons [72,73]. Therefore, it is specified that the best quantity of BC exists which harmonizes the visible light absorbance and photogenerated charge separation, subsequently improving the photodegradation efficiency of the BGCN composite which is assessed through the removal of CIP.

Based on the experimental results and study, the mechanism of photodegradation of CIP is well documented in many research works [74,75].

Recently, research work done by [76], determining the transformation of CIP into quite a lot of transitional species because of a photocatalytic procedure and acknowledged two degradation pathways, which endure sequences of reactions before the final mineralization of pollutants into H_2O and CO_2. The two-degradation mechanisms reported the loss of the carbonyl group in the quinoline ring structure followed by ring opening reactions by attack of $O_2^{\bullet -}$ and $OH^{\bullet}$ and cleavage of the piperazine ring through hydroxylation of CIP again by attack of $O_2^{\bullet -}$ and $OH^{\bullet}$. Both these mechanisms make reactive transitional species which after many reactions transform into H_2O and CO_2 at a later stage [76].

Reactions from 4 to 10 and Fig. 12 represent the proposed degradation mechanism for the degradation of CIP. Fig. 12 clearly shows the reduction of the band gap through the trapping and generation of electrons in a doped carbon interface acting as a sensitizer. This carbon sensitizer absorbs light and transfers an electron to the surface of the conduction band not only enhancing visible light absorbance through increased injection of high-energy electrons but also reducing electron-hole pair recombination [58]. It is understood that BC enhances visible light absorbance and charge separation by providing good sensitization, surface area, and conductive pathways for the reactive species. The electrons generated by photons in CB and at energy levels lessened O_2 to $O_2\bullet^-$. On the other hand, holes in the valence band oxidized H_2O and OH^- to OH• where H_2O_2 is produced by superoxide radicles reacting with H^+. Both species reacted with CIP adsorbed on the surface of BC or in solution to form numerous transitional reactive species which eventually resulted in the removal of CIP. The generation of these reactive oxygen species (ROS) is further confirmed through scavenger experiments employing photocatalyst with the best activity i.e. 0.22-BGCN. Fig. 13 represents the reduction in CIP concentration for all three scavengers used. As the scavengers are added the degradation rate of CIP is reduced due to the capturing effect of these scavenging agents and a CIP degradation rate of 51% is observed for EDTA. Likewise, the degradation rate for ethanol and IPA is 44% and 34%. The reduction in the degradation efficiency indicates the generation and capture of ROS by scavenging agents providing potential clues regarding the hydroxyl radicals OH• and superoxide radicles $O_2\bullet^-$ as the primary ROS in the degradation of CIP [77,78]. Henceforth, based on established literature, numerous reactions are tangled in the photocatalytic removal of CIP and are shown in equations 4-9 [79,80].

$$BCN \xrightarrow{hv} BCN\ (e_{CB}^-) + BCN\ (h_{VB}^+) \quad (4)$$

$$BCN(e_{CB}^-) + O_2 \rightarrow O_2^{\bullet -} \quad (5)$$

$$2O_2^{\bullet-} + 4H^+ \rightarrow 2H_2O_2 \quad (6)$$

$$BCN(h_{VB}^+) + OH^- \rightarrow OH^\bullet + BCN \quad (7)$$

$$CIP + OH^\bullet \rightarrow CO_2 + H_2O + Degradation\ products \quad (8)$$

$$CIP + O_2^{\bullet-} \rightarrow CO_2 + H_2O + Degradation\ products \quad (9)$$

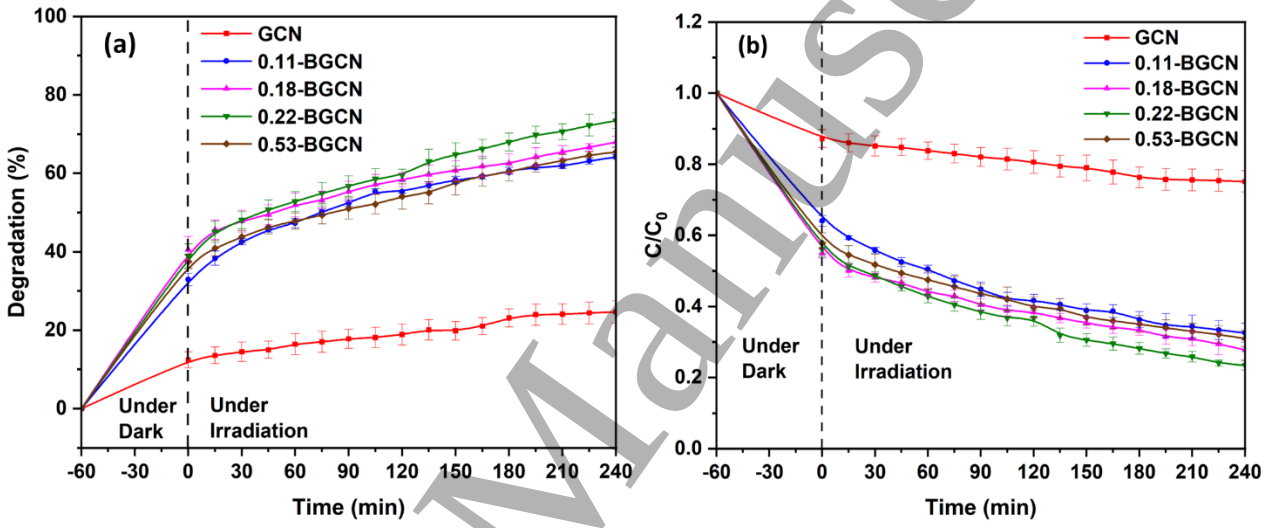

Figure 11. Assessment of the photocatalytic activity of GCN and *x*-BGCN samples verified by (a) degradation efficiency and (b) change in concentration of CIP micropollutant.

Table 5. Tabular representation of rate constants calculated on the basis of pseudo-first kinetics.

Sample name	Rate constant, *k* (min^{-1})
GCN	*0.000882*
0.11-BGCN	*0.00435*
0.18-BGCN	*0.00458*
0.22-BGCN	*0.00512*

0.53-BGCN	*0.00420*

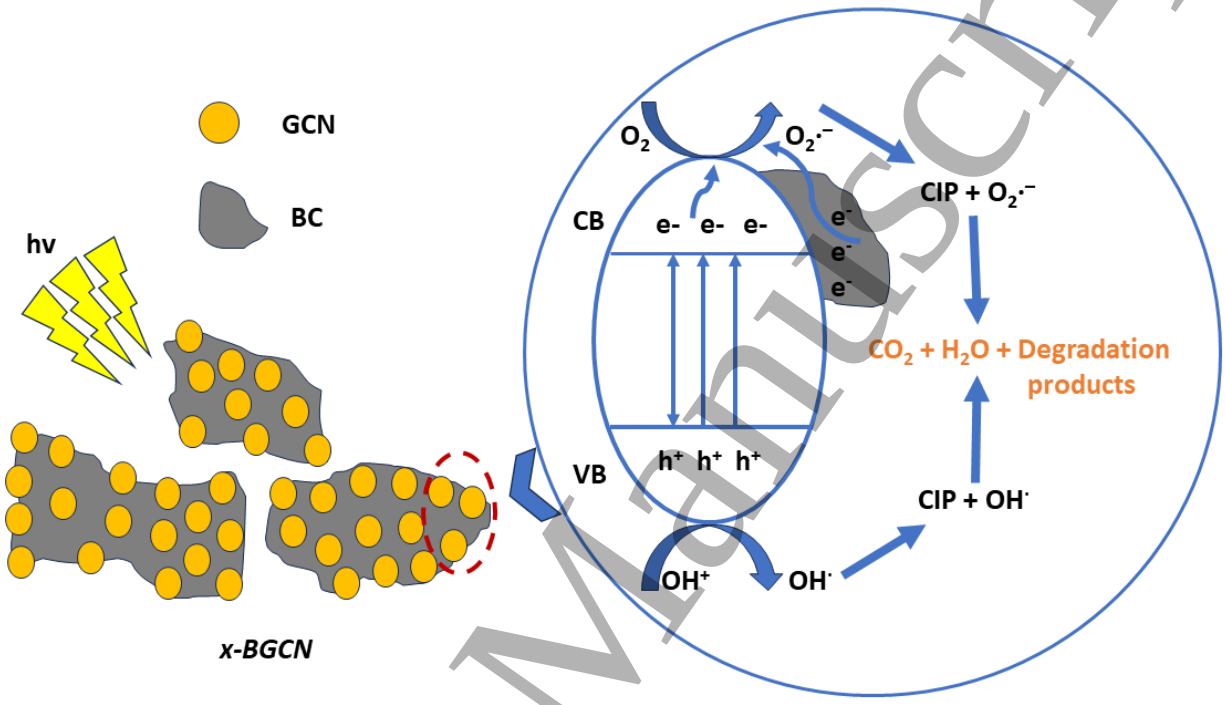

Figure 12. Suggested degradation mechanism of the photo-assisted removal of CIP micropollutant.

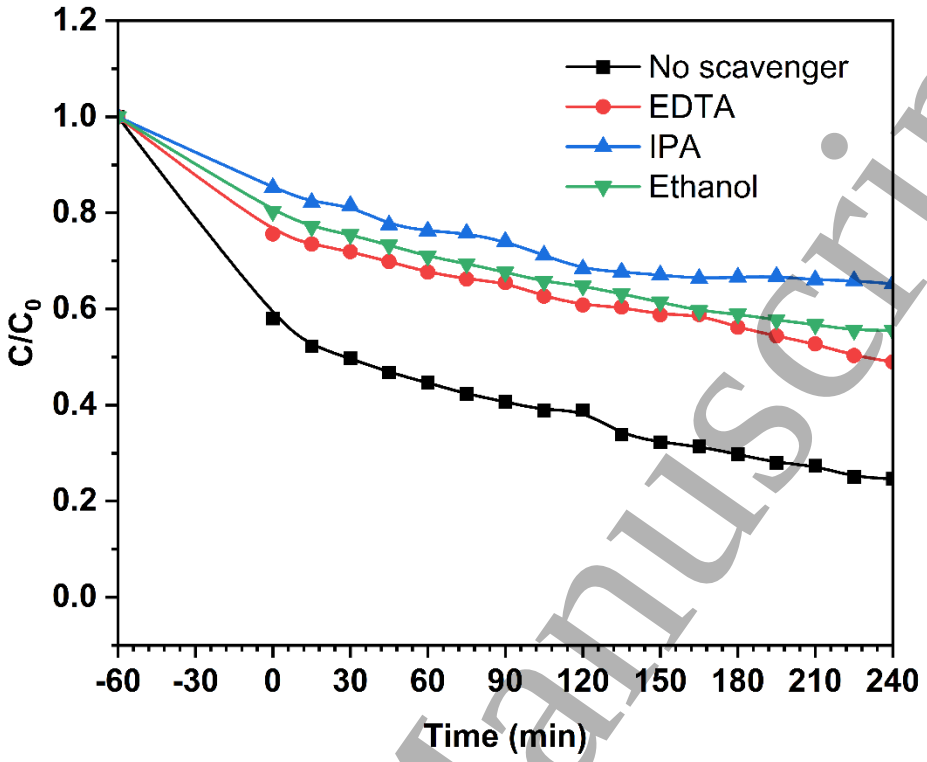

Figure 13. Scavenger effect of EDTA, IPA, and Ethanol on the concentration of CIP using 0.22-BGCN sample.

Table 6 is shown below which highlights better advantages of our prepared photocatalyst with some recently researched material in terms of light source and degradation rate of different pollutants. This table shows the enhanced efficiency of prepared composites towards photocatalysts degrading various pollutants under high-power light sources which indicates a keen will to develop a sustainable photocatalyst that is green and environment-friendly using BC and a 5W LED light source.

Table 6. Comparison of different biochar-based GCN composite photocatalysts with *x*-BGCN composite in terms of pollutant, light source, and degradation efficiency.

Photocatalyst	**Light source**	**Degradation efficiency**	**Pollutant**	**Citations**
Biochar/GCN composite (*x*-BGCN)	LED white light 5W	75 %	CIP	Present work
Graphitic carbon nitride/ biochar composite	500 W Xenon lamp with UV cutoff filter	81.1 %	Enrofloxacin	[40]
Biochar-based supramolecular self-assembled g-C_3N_4	250 W High-pressure sodium lamps	76.72 %	Phenanthrene	[81]
Graphene-like biochar/g-C_3N_4 without activated peroxymonosulfate	50 W (PLS-SXE300D/300DUV) Xenon lamp	70%	Tetracycline	[82]
BC/g-C_3N_4 composite	500 W Xenon Lamp	83 %	Tetracycline	[53]
Biochar skeleton and	250 W Xenon high-pressure mercury lamp	84.63 %	Formaldehyde	[83]

"chrysanthemum"
g-C_3N_4

4. Conclusions

Composite photocatalysts of biochar (BC) and graphitic carbon nitride (GCN) were prepared effectively using a simplistic preparation strategy targeting improved photocatalytic performance. The photocatalytic efficiency of the various composite samples of BC and GCN (*x*-BGCN), with different amounts of BC, was assessed for the photocatalytic removal of CIP. A 5 W LED light was used to assess the photocatalytic removal of CIP. The specimen having an optimized quantity of BC, i.e. 0.22-BGCN showed the best photodegradation efficiency. The enhanced photocatalytic activity after BC addition was attributed to the collective outcome of enhanced visible light absorbance and good electron-hole pair separation due to BC acting as a charge mediator. Augmented BC content resulted in a maximum performance to a certain limit and further increase in BC content decreased the photocatalytic efficiency. The narrowing of the band gap because of energy states resulted in enhanced visible light absorbance. On the contrary, a reduction of emission spectra is related to the insnaring and recombination of non-radiative photoexcited charges at energy levels in the case of 0.11 BGCN to 0.22 BGCN samples. The decrease in photocatalytic activity on further addition of BC is because of carbon blocking light irradiations to the GCN photocatalyst. The parameters like initial concentration and pH also showed an effect on the degradation efficiency of CIP whereas a low initial concentration and an acidic and basic pH level showed enhanced degradation efficiency of CIP using 0.22-BGCN composite. Likewise, the scavenger experiments were carried out to confirm the generation of ROS which proved the presence of OH• and $O_2^{\bullet -}$ as the primary ROS degrading CIP. Irrefutably, a facile preparation approach of BC-loaded GCN is proposed aiming at an environmentally welcoming, visible light-

driven, narrow band gap photocatalyst. This simple synthesis approach through the cost-effective loading of BC on GCN offered promising outcomes in the current research work. It is anticipated that this research will provide a basis for the economic development of visible light active (VLA) photocatalysts with enhanced productivity in terms of pharmaceutical micropollutant degradation.

Authors contribution

Ijlal Idrees: Experimentation, Investigation, Writing Draft ; **Muhammad Zafar:** Conceptualization, Writing, Review and Editing, Funding ; **Malik Adeel Umer:** Writing, Review and Editing ; **Amna Mir:** Review and Editing ; **Fahad Rehman, Abrar Faisal:** Experimentation and Formal Analysis ; **Abdul Razzaq:** Conceptualization, Methodology, Supervision, Writing, Review and Editing, Funding ; **Woo Young Kim:** Supervision, Writing, Review and Editing, Funding

Funding: The Higher Education Commission (HEC), Pakistan supported partially under the Startup Research Grant for Fresh PhD Holders, Project No. 21-1952/SRGP/R&D/HEC/2018. Also, this research was funded by “Regional Innovation Strategy (RIS)” through the National Research Foundation of Korea (NRF) funded by the Ministry of Education (MOE) (2023-RIS009).

Acknowledgement: The authors would like to thank Dr. Omar Awayssa from United Arab Emirates University for his assistance in characterizing the results of this experiment.

Data availability statement: Data are contained within the article.

Conflicts of Interest: The author declares no conflicts of interest.

References

[1] Duarte E D V, Oliveira M G, Spaolonzi M P, Costa H P S, Silva T L d., Silva M G C d. and Vieira M G A 2022 Adsorption of pharmaceutical products from aqueous solutions on functionalized carbon nanotubes by conventional and green methods: A critical review *J. Clean. Prod.* **372** 133743

[2] Chen Y, Yang J, Zeng L and Zhu M 2022 Recent progress on the removal of antibiotic pollutants using photocatalytic oxidation process *Crit. Rev. Environ. Sci. Technol.* **52** 1401–48

[3] Liu D, Xu Y Y, Junaid M, Zhu Y G and Wang J 2022 Distribution, transfer, ecological and human health risks of antibiotics in bay ecosystems *Environ. Int.* **158** 106949

[4] Silori R, Shrivastava V, Mazumder P and Kumar M 2023 Antimicrobial resistance surge in the context of pollution, war, and pandemic *Curr. Opin. Environ. Sci. Heal.* **34** 100479

[5] Zafar R, Bashir S, Nabi D and Arshad M 2021 Occurrence and quantification of prevalent antibiotics in wastewater samples from Rawalpindi and Islamabad, Pakistan *Sci. Total Environ.* **764** 142596

[6] Johansson C H, Janmar L and Backhaus T 2014 Toxicity of ciprofloxacin and sulfamethoxazole to marine periphytic algae and bacteria *Aquat. Toxicol.* **156** 248–58

[7] Ricky R and Shanthakumar S 2023 An investigation on removal of ciprofloxacin and norfloxacin by phycoremediation with an emphasis on acute toxicity and biochemical composition *Sci. Rep.* **13** 1–16

[8] Cheng N, Wang B, Chen M, Feng Q, Zhang X, Wang S, Zhao R and Jiang T 2023

Adsorption and photocatalytic degradation of quinolone antibiotics from wastewater using functionalized biochar *Environ. Pollut.* **336** 122409

[9] Chen Z, He Z, Zhou M, Xie M, He T, Zhao Y, Chen X, Wu Y and Xu Z 2021 In-situ synthesis of biochar modified PbMoO4: An efficient visible light-driven photocatalyst for tetracycline removal *Chemosphere* **284** 131260

[10] Asif M, Zafar M, Akhter P, Hussain M, Kim W Y, Umer A and Razzaq A 2021 Effect of urea addition on anatase phase enrichment and nitrogen doping of tio2 for photocatalytic abatement of methylene blue *Appl. Sci.* **11** 1–15

[11] Wongso V, Chen C J, Razzaq A, Kamal N A and Sambudi N S 2019 Hybrid kaolin/TiO2 composite: Effect of urea addition towards an efficient photocatalyst for dye abatement under visible light irradiation *Appl. Clay Sci.* **180** 105158

[12] Liu M, You W, Lei Z, Zhou G, Yang J, Wu G, Ma G, Luan G, Takata T, Hara M, Domen K and Li C 2004 Water reduction and oxidation on Pt-Ru/Y2Ta2O 5N2 catalyst under visible light irradiation *Chem. Commun.* 2192–3

[13] Liu K, Zhang C, Sun Y, Zhang G, Shen X, Zou F, Zhang H, Wu Z, Wegener E C, Taubert C J, Miller J T, Peng Z and Zhu Y 2018 High-Performance Transition Metal Phosphide Alloy Catalyst for Oxygen Evolution Reaction *ACS Nano* **12** 158–67

[14] Bukhari S A S, Zafar M, Mazhar F, Ahmed A, Fazal T, Rehman F, Razzaq A and Kim W Y 2024 Development of nickel doped graphitic carbon nitride (GCN) photocatalyst for enhanced degradation of textile pollutant under visible light irradiation *J. Saudi Chem. Soc.* **28** 101801

[15] Kim H R, Razzaq A, Grimes C A and In S Il 2017 Heterojunction p-n-p Cu2O/S-TiO2/CuO: Synthesis and application to photocatalytic conversion of CO2 to methane *J. CO2 Util.* **20** 91–6

[16] Zubair M, Razzaq A, Grimes C A and In S Il 2017 Cu2ZnSnS4 (CZTS)-ZnO: A noble metal-free hybrid Z-scheme photocatalyst for enhanced solar-spectrum photocatalytic conversion of CO2 to CH4 *J. CO2 Util.* **20** 301–11

[17] Chen D, Zhang X and Lee A F 2015 Synthetic strategies to nanostructured photocatalysts for CO2 reduction to solar fuels and chemicals *J. Mater. Chem. A* **3** 14487–516

[18] Fazal T, Razzaq A, Javed F, Hafeez A, Rashid N, Amjad U S, Ur Rehman M S, Faisal A and Rehman F 2020 Integrating adsorption and photocatalysis: A cost effective strategy for textile wastewater treatment using hybrid biochar-TiO2 composite *J. Hazard. Mater.* **390** 121623

[19] Asif M, Saeed M, Zafar M, Amjad U e. S, Razzaq A and Young Kim W 2022 Development of Co-Al LDH/GO composite photocatalyst for enhanced degradation of textile pollutant under visible light irradiation *Results Phys.* **42** 105997

[20] Singh P P and Srivastava V 2022 Recent advances in visible-light graphitic carbon nitride (g-C3N4) photocatalysts for chemical transformations *RSC Adv.* **12** 18245–65

[21] Cao S, Low J, Yu J and Jaroniec M 2015 Polymeric Photocatalysts Based on Graphitic Carbon Nitride *Adv. Mater.* **27** 2150–76

[22] Wang M, Cai Y, Zhou B, Yuan R, Chen Z and Chen H 2022 Removal of PFASs from water by carbon-based composite photocatalysis with adsorption and catalytic properties:

A review *Sci. Total Environ.* **836** 155652

[23] Zhang X, Bhattacharya T, Wang C, Kumar A and Nidheesh P V 2023 Straw-derived biochar for the removal of antibiotics from water: Adsorption and degradation mechanisms, recent advancements and challenges *Environ. Res.* **237** 116998

[24] Rasouli K, Rasouli J, Mohtaram M S, Sabbaghi S, Kamyab H, Moradi H and Chelliapan S 2023 Biomass-derived activated carbon nanocomposites for cleaner production: A review on aspects of photocatalytic pollutant degradation *J. Clean. Prod.* **419** 138181

[25] Li J, Yu G, Pan L, Li C, You F, Xie S, Wang Y, Ma J and Shang X 2018 Study of ciprofloxacin removal by biochar obtained from used tea leaves *J. Environ. Sci. (China)* **73** 20–30

[26] Wang G, Li Y, Dai J and Deng N 2022 Highly efficient photocatalytic oxidation of antibiotic ciprofloxacin using TiO2@g-C3N4@biochar composite *Environ. Sci. Pollut. Res.* **29** 48522–38

[27] Meng L, Yin W, Wang S, Wu X, Hou J, Yin W, Feng K, Ok Y S and Wang X 2020 Photocatalytic behavior of biochar-modified carbon nitride with enriched visible-light reactivity *Chemosphere* **239** 124713

[28] Shailendrakumar S, Chava R, Appari S, Bahurudeen A, Vardhan B and Kuncharam R 2022 Journal of Environmental Chemical Engineering Sustainable use of rice husk for the cleaner production of value-added products *J. Environ. Chem. Eng.* **10** 106899

[29] Sarwar A, Razzaq A, Zafar M, Idrees I, Rehman F and Kim W Y 2023 Copper tungstate (CuWO4)/graphene quantum dots (GQDs) composite photocatalyst for enhanced

degradation of phenol under visible light irradiation *Results Phys.* **45** 106253

[30] Krýsa J, Bouzek K and Stollberg C 2000 Photocatalytic degradation of oxalic acid on a semiconductive layer of n-TiO2 particles in a batch plate reactor. Part III: Rate determining steps and nonsteady diffusion model for oxygen transport *J. Appl. Electrochem.* **30** 1033–41

[31] Chakrabarti S and Dutta B K 2004 Photocatalytic degradation of model textile dyes in wastewater using ZnO as semiconductor catalyst *J. Hazard. Mater.* **112** 269–78

[32] Osagiede C A and Aisien F A 2024 Biochar-based bi-functional catalyst derived from rubber seed shell and eggshell for biodiesel production from waste cooking oil *Fuel* **358** 130076

[33] Derkani M H, Fletcher A J, Fedorov M, Abdallah W, Sauerer B, Anderson J and Zhang Z J 2019 Mechanisms of surface charge modification of carbonates in aqueous electrolyte solutions *Colloids and Interfaces* **3**

[34] Smýkalová A, Kinnertová E, Slovák V and Praus P 2023 Metal-free hybrid nanocomposites of graphitic carbon nitride and char: Synthesis, characterisation and photocatalysis under visible irradiation *J. Taiwan Inst. Chem. Eng.*

[35] Miroliaei M R, Dadfarma A, Shahabi-Nejad M, Jalali E and Sheibani H 2023 Biochar/g-C3N4 nano hetero-structure decorated with pt nanoparticles for diazinon photodegradation and E. coli photodeactivation under visible light *Brazilian J. Chem. Eng.*

[36] Wang R, Lan X, Zhou T, Qian X, Qu B, Lv P and Wang Y 2024 Detection of chloramphenicol in dairy products based on biogas residue biochar based electrochemical

sensor *J. Food Compos. Anal.* **125** 105824

[37] Xu C, Liu R, Chen L and Wang Q 2023 Efficient Adsorption Removal of Phosphate from Rural Domestic Sewage by Waste Eggshell-Modified Peanut Shell Biochar Adsorbent Materials *Materials (Basel).* **16**

[38] Zhang L, Jin Z, Huang S, Huang X, Xu B, Hu L, Cui H, Ruan S and Zeng Y J 2019 Bio-inspired carbon doped graphitic carbon nitride with booming photocatalytic hydrogen evolution *Appl. Catal. B Environ.* **246** 61–71

[39] Zheng Y, Yang Y, Zhang Y, Zou W, Luo Y, Dong L and Gao B 2019 Facile one-step synthesis of graphitic carbon nitride-modified biochar for the removal of reactive red 120 through adsorption and photocatalytic degradation *Biochar* **1** 89–96

[40] Xiao Y, Lyu H, Yang C, Zhao B, Wang L and Tang J 2021 Graphitic carbon nitride/biochar composite synthesized by a facile ball-milling method for the adsorption and photocatalytic degradation of enrofloxacin *J. Environ. Sci. (China)* **103** 93–107

[41] Yang J, Zhang M, Wang H, Xue J, Lv Q and Pang G 2021 Efficient recovery of phosphate from aqueous solution using biochar derived from co-pyrolysis of sewage sludge with eggshell *J. Environ. Chem. Eng.* **9**

[42] Bansod N D, Roy K, Das C, Vidyasagar D and Potiyaraj P 2019 Development and characterization of graphitic carbon nitride as nonblack filler in natural rubber composites *J. Appl. Polym. Sci.* **136** 1–8

[43] Li X, Zhang J, Shen L, Ma Y, Lei W, Cui Q and Zou G 2009 Preparation and characterization of graphitic carbon nitride through pyrolysis of melamine *Appl. Phys. A*

Mater. Sci. Process. **94** 387–92

[44] Tong Z, Hai Y, Wang B, Lv F, Zhong Z and Xiong R 2023 Activated g-C3N4 Photocatalyst with Defect Engineering for Efficient Reduction of CO2in Water *J. Phys. Chem. C* **127** 11067–75

[45] Dahiya S, Sharma A and Chaudhary S 2023 Synthesis of phytoextract-mediated Ag-doped graphitic carbon nitride (Ag@GCN) for photocatalytic degradation of dyes *Environ. Sci. Pollut. Res.* **30** 25650–62

[46] Buu T T, Hai N D, Cong C Q, Nam N T H, Khoa T D, Vy D G, Nguyen N T, Oanh D T Y and Hieu N H 2024 A case study of different bismuth oxyhalides BiOX (X = F, Cl, Br, and I)/biochar-derived rice husk@graphitic carbon nitride for the robustness of H2O2 photoproduction and antibiotic photodegradation *J. Water Process Eng.* **57** 104558

[47] Balakrishnan A, Chinthala M and Polagani R K 2024 3D kaolinite/g-C3N4-alginate beads as an affordable and sustainable photocatalyst for wastewater remediation *Carbohydr. Polym.* **323** 121420

[48] Xia P, Zhu B, Yu J, Cao S and Jaroniec M 2017 Ultra-thin nanosheet assemblies of graphitic carbon nitride for enhanced photocatalytic CO2 reduction *J. Mater. Chem. A* **5** 3230–8

[49] Bhanderi D, Lakhani P and Modi C K 2023 Graphitic carbon nitride (g-C3N4) as an emerging photocatalyst for sustainable environmental applications: a comprehensive review *RSC Sustain.* **2** 265–87

[50] Ma R, Sun Y, Zhang H, Zhu J, Tian H, Guo X, Wang R, Cui X, Hou X and An S 2024

Intense interaction between biochar/g-C3N4 promotes the photocatalytic performance of heterojunction catalysts *RSC Adv.* **14** 19707–17

[51] Cui J, Zhang F, Li H, Cui J, Ren Y and Yu X 2020 Recent progress in biochar-based photocatalysts for wastewater treatment: Synthesis, mechanisms, and applications *Appl. Sci.* **10**

[52] Karpuraranjith M, Chen Y, Ramadoss M, Wang B, Yang H, Rajaboopathi S and Yang D 2021 Magnetically recyclable magnetic biochar graphitic carbon nitride nanoarchitectures for highly efficient charge separation and stable photocatalytic activity under visible-light irradiation *J. Mol. Liq.* **326** 115315

[53] Guo F, Shi C, Sun W, Liu Y, Lin X and Shi W 2022 Pomelo biochar as an electron acceptor to modify graphitic carbon nitride for boosting visible-light-driven photocatalytic degradation of tetracycline *Chinese J. Chem. Eng.* **48** 1–11

[54] Jeon P, Lee M E and Baek K 2017 Adsorption and photocatalytic activity of biochar with graphitic carbon nitride (g-C3N4) *J. Taiwan Inst. Chem. Eng.* **77** 244–9

[55] Xie Y, Liu A, Bandala E R and Goonetilleke A 2022 TiO2-biochar composites as alternative photocatalyst for stormwater disinfection *J. Water Process Eng.* **48** 102913

[56] Xu Y and Gao S P 2012 Band gap of C3N4 in the GW approximation *Int. J. Hydrogen Energy* **37** 11072–80

[57] Brombilla V de L, Sarmento Lazarotto J, Silvestri S, Anschau K F, Dotto G L and Foletto E L 2022 Biochar derived from yerba-mate (Ilex paraguariensis) as an alternative TiO2 support for enhancement of photocatalytic activity toward Rhodamine-B degradation in

water *Chem. Eng. Commun.* **209** 1334–47

[58] Mian M M and Liu G 2018 Recent progress in biochar-supported photocatalysts: Synthesis, role of biochar, and applications *RSC Adv.* **8** 14237–48

[59] Das D, Banerjee D, Pahari D, Ghorai U K, Sarkar S, Das N S and Chattopadhyay K K 2017 Defect induced tuning of photoluminescence property in graphitic carbon nitride nanosheets through synthesis conditions *J. Lumin.* **185** 155–65

[60] Feng Z, Yuan R, Wang F, Chen Z, Zhou B and Chen H 2021 Preparation of magnetic biochar and its application in catalytic degradation of organic pollutants: A review *Sci. Total Environ.* **765** 142673

[61] Wu X, Gao D, Wang P, Yu H and Yu J 2019 NH4Cl-induced low-temperature formation of nitrogen-rich g-C3N4 nanosheets with improved photocatalytic hydrogen evolution *Carbon N. Y.* **153** 757–66

[62] Malakootian M, Nasiri A and Amiri Gharaghani M 2020 Photocatalytic degradation of ciprofloxacin antibiotic by TiO2 nanoparticles immobilized on a glass plate *Chem. Eng. Commun.* **207** 56–72

[63] Sayed M, Ismail M, Khan S, Tabassum S and Khan H M 2016 Degradation of ciprofloxacin in water by advanced oxidation process: Kinetics study, influencing parameters and degradation pathways *Environ. Technol. (United Kingdom)* **37** 590–602

[64] Fang Z, Lin Z, Chen P, Feng M, Liu H, Xiao Z, Lin Z, Li D, Liu D, Zhang Y, Lv W and Liu G 2023 Enhanced photochemical degradation and transformation of ciprofloxacin in a UV/calcium peroxide system: pH effects, defluorination kinetics, and different

components numerical analysis *J. Clean. Prod.* **414** 137706

[65] Decolorization P D Development of AgFeO 2 / rGO / TiO 2 Ternary Composite Photocatalysts for Enhanced Photocatalytic Dye Decolorization

[66] Bell S, Will G and Bell J 2013 Light intensity effects on photocatalytic water splitting with a titania catalyst *Int. J. Hydrogen Energy* **38** 6938–47

[67] Liu H, Ye C, Xu Y and Wang Q 2022 Effect of activation conditions and iron loading content on the catalytic cracking of toluene by biochar *Energy* **247** 123409

[68] Pi L, Jiang R, Zhou W, Zhu H, Xiao W, Wang D and Mao X 2015 G-C 3 N 4 Modified biochar as an adsorptive and photocatalytic material for decontamination of aqueous organic pollutants *Appl. Surf. Sci.* **358** 231–9

[69] Wang T, Dissanayake P D, Sun M, Tao Z, Han W, An N, Gu Q, Xia D, Tian B, Ok Y S and Shang J 2021 Adsorption and visible-light photocatalytic degradation of organic pollutants by functionalized biochar: Role of iodine doping and reactive species *Environ. Res.* **197** 111026

[70] Das R S, Warkhade S K, Kumar A, Gaikwad G S and Wankhade A V. 2020 Graphitic carbon nitride @ silver zirconate nanocomposite (gC3N4@Ag2ZrO3): A Type-II heterojunction for an effective visible light photocatalysis and bacterial photo-inactivation *J. Alloys Compd.* **846** 155770

[71] Tahir M, Sherryna A, Khan A A, Madi M, Zerga A Y and Tahir B 2022 Defect Engineering in Graphitic Carbon Nitride Nanotextures for Energy Efficient Solar Fuels Production: A Review *Energy & Fuels* **36** 8948–77

[72] Ye S, Yan M, Tan X, Liang J, Zeng G, Wu H, Song B, Zhou C, Yang Y and Wang H 2019 Facile assembled biochar-based nanocomposite with improved graphitization for efficient photocatalytic activity driven by visible light *Appl. Catal. B Environ.* **250** 78–88

[73] Kahkeci J and Gamal El-Din M 2023 Biochar-supported photocatalysts: Performance optimization and applications in emerging contaminant removal from wastewater *Chem. Eng. J.* **476** 146530

[74] Wang Z, Cai X, Xie X, Li S, Zhang X and Wang Z 2021 Visible-LED-light-driven photocatalytic degradation of ofloxacin and ciprofloxacin by magnetic biochar modified flower-like Bi2WO6: The synergistic effects, mechanism insights and degradation pathways *Sci. Total Environ.* **764** 142879

[75] Ao X, Liu W, Sun W, Cai M, Ye Z, Yang C, Lu Z and Li C 2018 Medium pressure UV-activated peroxymonosulfate for ciprofloxacin degradation: Kinetics, mechanism, and genotoxicity *Chem. Eng. J.* **345** 87–97

[76] Yan B, Chen G, Ma B, Guo Y, Zha Y, Li J, Wang S, Liu J, Zhao B and Xie H 2024 Construction of surface plasmonic Bi nanoparticles and α-Bi2O3 co-modified TiO2 nanotube arrays for enhanced photocatalytic degradation of ciprofloxacin: Performance, DFT calculation and mechanism *Sep. Purif. Technol.* **330** 125180

[77] Thi Mai N, Van Thanh D, Nhat Huy N, Danh Bich D, Thi Minh Hang T, Huu Hao N and Manh Khai N 2025 Red mud supported on rice husk biochar as sono-photo-Fenton catalysts for degradation of ciprofloxacin in water *Sep. Purif. Technol.* **354** 129039

[78] Toan T Q, Mai N T, Trang H M, Van Hao P and Van Thanh D 2023 Ultrasonic-assisted synthesis of magnetic recyclable Fe3O4/rice husk biochar based photocatalysts for

ciprofloxacin photodegradation in aqueous solution *RSC Adv.* **13** 11171–81

[79] Wang Z, Cai X, Xie X, Li S, Zhang X and Wang Z 2021 Visible-LED-light-driven photocatalytic degradation of ofloxacin and ciprofloxacin by magnetic biochar modified flower-like Bi2WO6: The synergistic effects, mechanism insights and degradation pathways *Sci. Total Environ.* **764**

[80] Amir M, Fazal T, Iqbal J, Din A A, Ahmed A, Ali A, Razzaq A, Ali Z, Rehman M S U and Park Y K 2022 Integrated adsorptive and photocatalytic degradation of pharmaceutical micropollutant, ciprofloxacin employing biochar-ZnO composite photocatalysts *J. Ind. Eng. Chem.* **115** 171–82

[81] Lin M, Li F, Cheng W, Rong X and Wang W 2022 Facile preparation of a novel modified biochar-based supramolecular self-assembled g-C3N4 for enhanced visible light photocatalytic degradation of phenanthrene *Chemosphere* **288** 132620

[82] Tang R, Gong D, Deng Y, Xiong S, Zheng J, Li L, Zhou Z, Su L and Zhao J 2022 π-π stacking derived from graphene-like biochar/g-C3N4 with tunable band structure for photocatalytic antibiotics degradation via peroxymonosulfate activation *J. Hazard. Mater.* **423** 126944

[83] Li X, Qian X, An X and Huang J 2019 Preparation of a novel composite comprising biochar skeleton and "chrysanthemum" g-C3N4 for enhanced visible light photocatalytic degradation of formaldehyde *Appl. Surf. Sci.* **487** 1262–70